© 2019. Published by The Company of Biologists Ltd | Development (2019) 146, dev181917. doi:10.1242/dev.181917

STEM CELLS AND REGENERATION

RESEARCH ARTICLE

Prediction and control of symmetry breaking in embryoid bodies by environment and signal integration

Naor Sagy, Shaked Slovin, Maya Allalouf, Maayan Pour, Gaya Savyon, Jonathan Boxman and Iftach Nachman*

ABSTRACT

During early embryogenesis, mechanical constraints and localized biochemical signals co-occur around anteroposterior axis determination and symmetry breaking. Their relative roles, however, are hard to tease apart *in vivo*. Using brachyury (Bra), a primitive streak and mesendoderm marker in mouse embryoid bodies (EBs), we studied how contact, biochemical cues and neighboring cell cues affect the positioning of a primitive streak-like locus and thus determine the anteroposterior axis. We show that a Bra-competent layer must be formed in the EB before Bra expression initiates, and that Bra onset locus position is biased by contact points of the EB with its surrounding, probably through modulation of chemical cues rather than by mechanical signaling. We can push or pull Bra onset away from contact points by introducing a separate localized Wnt signal source, or maneuver Bra onset to a few loci or to an isotropic peripheral pattern. Furthermore, we show that Foxa2-positive cells are predictive of the future location of Bra onset, demonstrating an earlier symmetry-breaking event. Our analysis of factors affecting symmetry breaking and spatial fate choice during this developmental process could prove valuable for *in vitro* differentiation and organoid formation.

KEY WORDS: Brachyury, Embroid bodies, Gastruloids, Organoids, Symmetry breaking, Mouse

INTRODUCTION

In the early mouse embryo, the blastocyst implants into the uterus wall on the fourth day of gestation. A series of events follows, including formation of an anteroposterior (AP) axis initiated by the localization of anterior visceral endoderm (AVE) cells at the prospective anterior side and emergence of the primitive streak at the posterior side (Arnold and Robertson, 2009). The primitive streak is formed through interaction between BMP, Nodal, FGF and Wnt pathways at the posterior side of the blastocyst and is limited to that side by inhibitory signals originating from the AVE at the anterior side (Arnold and Robertson, 2009; Robertson, 2005). Mechanical pressure, presumably stemming from the uterus wall, was suggested to be necessary for proper AP axis formation, including positioning of the AVE and elongation of the egg cylinder (Hiramatsu et al., 2013), although this dependence was later challenged (Bedzhov et al., 2015). Mechanical strain associated with gastrulation was also demonstrated to drive mesoderm specification in fish, fly and sea anemones through modification of β-catenin (Brunet et al., 2013; Pukhlyakova et al., 2018). Another factor shaping primitive streak and AP axis formation is the visceral endoderm layer, characterized at embryonic day (E)5.5 by the expression of Foxa2. As mechanical signals, localized biochemical signals and neighboring cell layer contexts all co-occur in a specific reproducible pattern during embryogenesis, it is very hard to dissect their respective roles and dependencies in specifying primitive streak location selection and axis formation.

In vitro multicellular models such as embryoid bodies (EBs), and gastruloids derived from EBs, have been used in recent years to dissect certain aspects of early embryonic development (Poh et al., 2014; Turner et al., 2014; van den Brink et al., 2014; Warmflash et al., 2014). These models are formed by 3D aggregation of pluripotent stem cells. Given proper conditions, these aggregates differentiate in a partially organized manner, break their radial symmetry and develop an AP axis (Beccari et al., 2018; ten Berge et al., 2008; van den Brink et al., 2014). Interestingly, when aggregated from a small number of cells and under specific signal conditions, EBs form ‘gastruloids’, which display not only initial symmetry breaking but multiple axes as well as elongation (Turner et al., 2017; van den Brink et al., 2014). Germ layer structure was also shown in confined 2D colonies (Etoc et al., 2016; Morgani et al., 2018; Warmflash et al., 2014). Furthermore, by mixing mouse embryonic stem cells (mESCs) with extra-embryonic cells it is possible to obtain *in vitro* structures that resemble early stage mouse embryos in terms of both gene expression profile and morphology, including dual axis formation (Harrison et al., 2017; Sozen et al., 2018). The success of these *in vitro* structures in capturing some of the spatiotemporal aspects of early embryogenesis make them valuable model systems for studying the basic principles of early development, in addition to strategies of *in vitro* differentiation and tissue engineering. One of the earliest fate decisions that can be observed in embryonic stem cells is their differentiation to mesendoderm progenitors, which are characteristic of the primitive streak and are marked by brachyury (Bra; also known as T) (Gadue et al., 2006; Kubo et al., 2004; Tada et al., 2005). In 2D patterned colonies, the biased onset pattern of Bra has been associated with colony geometry as well as cell density (Blin et al., 2018). In 3D models such as EBs and gastruloids, the polar onset pattern of Bra expression provides one of the first detectable events of symmetry breaking (Beccari et al., 2018; Blin et al., 2018; Boxman et al., 2016; ten Berge et al., 2008; van den Brink et al., 2014). The mechanisms leading to the spatial selection of this pole and axis formation in these 3D models are, however, not clear.

Here we show that the onset of Bra expression is influenced by contact in EBs. Although the entire EB outer shell has the potential to express Bra, expression of this regulator is initiated at the point of EB contact with its surrounding surface. By manipulating the EB environment, we were able to alter the onset of Bra expression to multiple loci, a wide contact surface or an isotropic pattern

Department of Biochemistry and Molecular Biology, Tel Aviv University, Tel Aviv 6997801, Israel.

*Author for correspondence (iftachn@tauex.tau.ac.il)

M.P., 0000-0003-1997-5193; I.N., 0000-0002-4667-0398

Received 24 June 2019; Accepted 16 September 2019

Development (2019) 146, dev181917. doi:10.1242/dev.181917

throughout the outer shell. By creating spatially separate sources of contact and biochemical signals, we could demonstrate how the tissue can integrate these two modalities to define a single Bra locus. Remarkably, Foxa2 appeared with an eccentric bias toward the future onset site of Bra, evident of an earlier symmetry-breaking event and revealing different dependencies on Wnt signaling.

Our findings provide insight into symmetry-breaking mechanisms in 3D tissue models and primitive streak spatial selection *in utero*, demonstrating how contact and biochemical signals could integrate to drive symmetry breaking and mesendoderm differentiation.

RESULTS

Brachyury expression onset location in EBs is influenced by contact

We have previously observed that in EBs differentiated within agarose microwells in the absence of strong Wnt activation, Bra expression predominantly starts from a single locus on the EB external shell and spreads in that layer toward the opposite pole, where a locus is defined as a cluster of Bra-positive cells (see Materials and Methods) (Boxman et al., 2016). However, it is unclear whether the spatial selection of the locus is an outcome of stochastic symmetry breaking within the EB and why Bra expresion starts solely on the outer shell and not in the volume. Mouse E14 Bra-GFP ESCs (Fehling et al., 2003) pre-grown in serum and leukemia inhibitory factor (serum-LIF) were suspended in differentiation medium, aggregated into EBs in hanging drops for 24 h and then seeded in agarose microwell arrays for live imaging up to the onset of Bra-GFP expression (∼72 h), or differentiated within the hanging drops for a similar period (Fig. 1A). In EBs differentiated in agarose microwells, Bra expression commenced from the contact point of EBs with the wall or floor of the microwell (Fig. 1B-F; Movies 1-4). Out of 47 successfully imaged EBs, 16 showed Bra onset at the bottom of the well, 12 showed side onset, 14 showed joint side and bottom onset (Fig. 1C) and five showed two disparate onset loci. We noted that side-onset or dual-onset EBs were generally larger than bottom onset EBs (mean EB radius 120 µm, σ=16 µm, versus mean radius 95 µm, σ=17 µm, P=0.001), raising the hypothesis that side onset is driven by contact with the side wall, which is more common in larger EBs. This was reinforced by examining EBs with two Bra loci, which touched the microwell boundaries at two points or a large surface area overlapping the onset loci (Fig. 1D). We therefore compared in a separate experiment the onset angles in bottom-only contact EBs (n=9) with EBs touching the side wall (n=10) and found a significant difference, indicating that onset location is affected by contact [P=3e–5, two-sample Kolmogorov–Smirnov (KS) test; Fig. 1F]. Interestingly, EBs differentiated in hanging drops also displayed a single locus Bra pattern (Fig. 2B). Because EBs grown in hanging drops lie at the drop's bottom boundary, we hypothesized that their onset is also biased toward this boundary. The alternative result would be random spatial onset, caused by either lack of an organizing event or random rotations of the EB in the drop. Analyzing the locus location in hanging drops (n=12, P=1e–5, KS test), we found that the locus of Bra onset was at the bottom, similar to the bottom-contact EBs grown in microwells (Fig. 1F). Taken together, the results indicate that both mechanical contact and confinement by the liquid-to-air interface can determine the onset location of Bra in EBs. Such contact dependence could be explained by signal consolidation around the contact interface and/or by mechanosensing pathways.

We next wanted to check whether the timing and location of Bra onset can be controlled by imposing contact at a specific locus at an early stage. To this end, we fabricated 200 µm wide rectangular 'micropool' structures to enforce early contact at two sides of the EB (Fig. 1G,H). Of the EBs grown in these micropools, 30/41 touched the micropool walls and 11/41 contacted only the well bottom. In the side-contacting group, 29/30 expressed Bra at their side-contact points, compared with 2/11 nontouching EBs with side onset (P<1e–5, Fisher's exact test; Movies 5 and 6). Out of the side-contact, side-onset EBs, 26/29 showed a single locus onset (Fig. 1G) and 3/29 showed simultaneous onset at two loci (Fig. 1H). The preference of one side might result from earlier Bra triggering on that side as a result of faster signal consolidation, allowing enough time for the signal to spread toward the other side and mask or prevent the formation of a second locus. EBs grown in wider micropools (500 µm width) and which did not touch the walls showed bottom Bra expression onset at the contact point with the plate floor (8/10), similar to the case in large microwells (n>50 in multiple experiments; Boxman et al., 2016). We then evaluated the effect of early contact on the timing of Bra onset. When grown in the narrow (200 µm) micropools, EBs created contact with the micropool sides earlier (50–60 h), but Bra onset did not occur earlier than for nontouching controls in the wide micropools (79 h, σ=2 h, n=11 versus 75 h, σ=5 h, n=5). This suggests that cells on the outer shell of the EB did not yet have the potential to express Bra when contact was initially applied to the EB, and more molecular changes had to take place before Bra onset could occur around the contact point.

A Bra-competent shell is formed prior to onset

The observation that EBs can form multiple contact loci or an entire cap contact locus when confined in micropools raised the question of whether the potential to express Bra is limited to specific areas on the outer layer of the EB, to the entire shell, or is uniform throughout the EB volume. Growing EBs in hanging drops, we first confirmed that a canonical Wnt activation reporter (SuTOP-CFP) (Serup et al., 2012) showed colocalization with Bra, in agreement with observations that Bra is activated via the canonical Wnt pathway (Fig. S1A) (Arnold et al., 2000; ten Berge et al., 2008). We then tested EB spatial limitations for Bra onset under external Wnt induction. To this end, we induced the canonical Wnt pathway by adding the small-molecule Wnt pathway agonist CHIR99021 (CHIR) bypassing the pathway receptor via Gsk3β inhibition, adding soluble Wnt3a ligand or embedding Wnt3a-coated beads within the entire EB volume during aggregation (Fig. S1B) (Habib et al., 2013). EBs under CHIR treatment showed isotropic onset with no distinct locus, suggesting that the entire outer shell was Bra competent (n=16/16; Fig. 2B, center). Activation by soluble Wnt3a resulted in a stronger, yet polarized, locus (n=10/10; Fig. 2B, right) (ten Berge et al., 2008). EBs embedded with Wnt3a beads from aggregation displayed isotropic or near isotropic Bra expression onset on the outer shell at 72 h, similar to CHIR-treated EBs, which can be attributed to multiple loci caused by different beads (Fig. S1C). As in our forced early contact results, Wnt3a beads did not lead to Bra expression until 72 h after aggregating the EBs, nor did they induce Bra under pluripotency conditions (Fig. S1B, left). These results confirm that, similar to their susceptibility to contact, outer-layer cells need to reach a certain maturation stage before becoming Wnt-susceptible to activate Bra.

As the entire outer shell is Bra competent and contact is associated with the Bra onset locus, we hypothesized that once given uniform contact conditions, outer layer cells will induce Bra in a spherically isotropic pattern. We therefore tested the Bra onset pattern when EBs

Development (2019) 146, dev181917. doi:10.1242/dev.181917

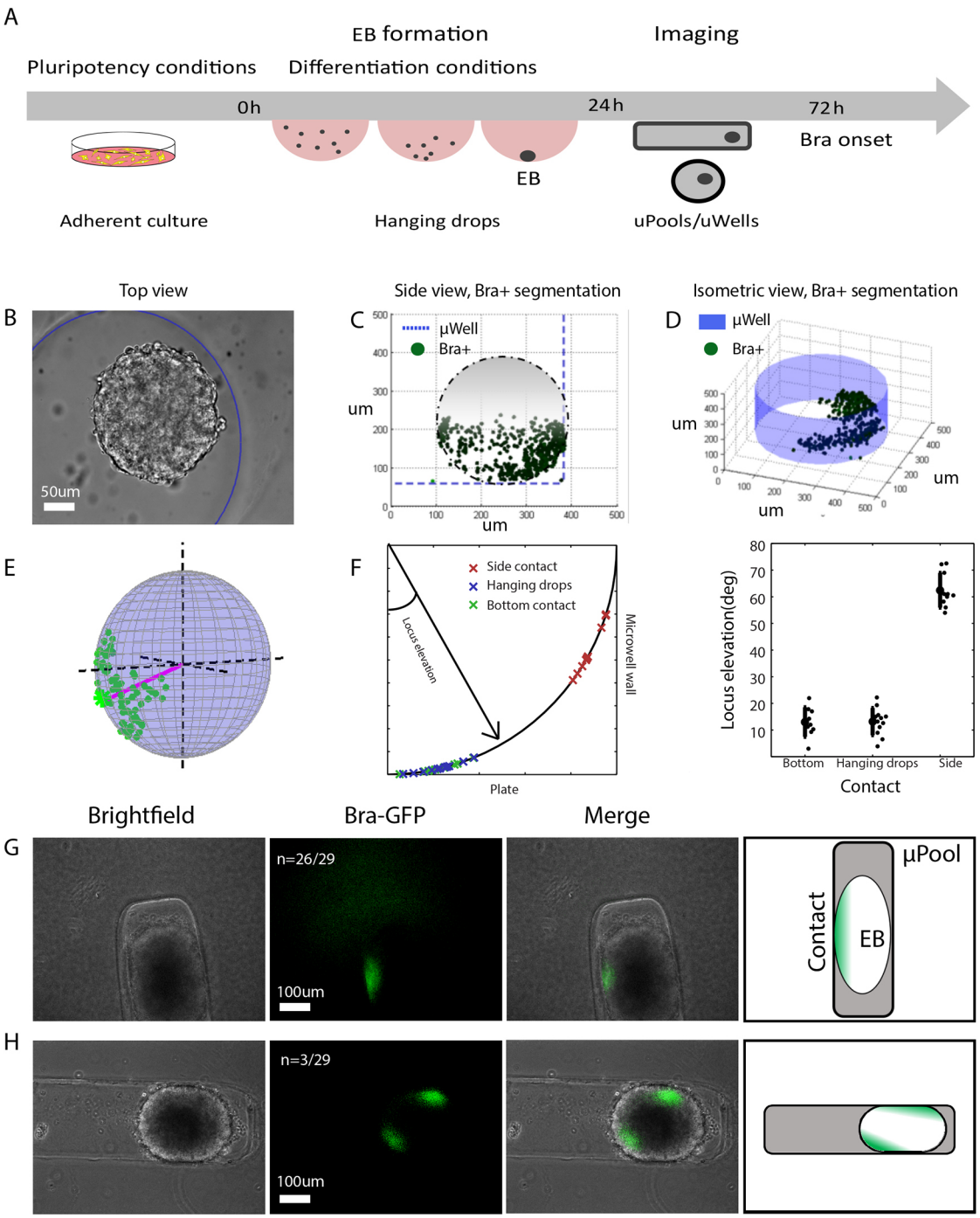

Fig. 1. Bra activation is influenced by contact. (A) Scheme of microwell and micropool experiments. (B) An EB in a microwell at 72 h after aggregation. Microwell walls are outlined with a blue circle. (C) Segmented Bra signal for the EB in B, at sagittal view aspect, showing Bra onset from the contact. (D) An EB touching the well walls at two points. Bra onsets from both points. (E) Estimation of the spatial location of Bra locus on segmentation data. The locus vector is shown in magenta. The blue sphere denotes the full EB volume. (F) Locus elevation angle for EBs with bottom contact only (green marks) or side contact (red marks) as determined from the brightfield channel at 60 h, as well as for EBs differentiated and imaged in hanging drops at 72 h (blue marks). EBs are depicted on a quarter circle (left) or as mean±s.d. (right). Locus elevation is largely determined by contact point. For bottom onset, the locus angle is biased upwards due to asymmetric expansion of Bra-positive cells in azimuth. For side onset, the locus angle is biased downwards due to the positive slope of the microwell walls. EBs with dual side and bottom locus were omitted from the analysis for visual clarity. (G,H) Enforcing contact points by growing EBs in narrow micropools (200 µm wide) affects Bra locus locations. Examples of a single side locus (G) and double side loci (H) are shown.

were differentiated while embedded in rich ECM composition (Matrigel) or in a more biologically inert hydrogel (low gelling point agarose). When embedded in Matrigel, EBs in a range of sizes displayed isotropic onset patterns (13/15, mean radius at onset 95 µm, σ=50 µm), whereas two large EBs (radii of 120 and 180 µm) initiated Bra from a distinct locus (Fig. 2C; Movies 7 and 8). To test whether the effect of Matrigel was mainly a result of mechanical pressure or of biochemical interactions with its components, we tested the dynamics for EBs embedded in low melting point agarose of lower (0.5%), similar (1%) or higher (1.5%) stiffness than Matrigel. EBs embedded

Development (2019) 146, dev181917. doi:10.1242/dev.181917

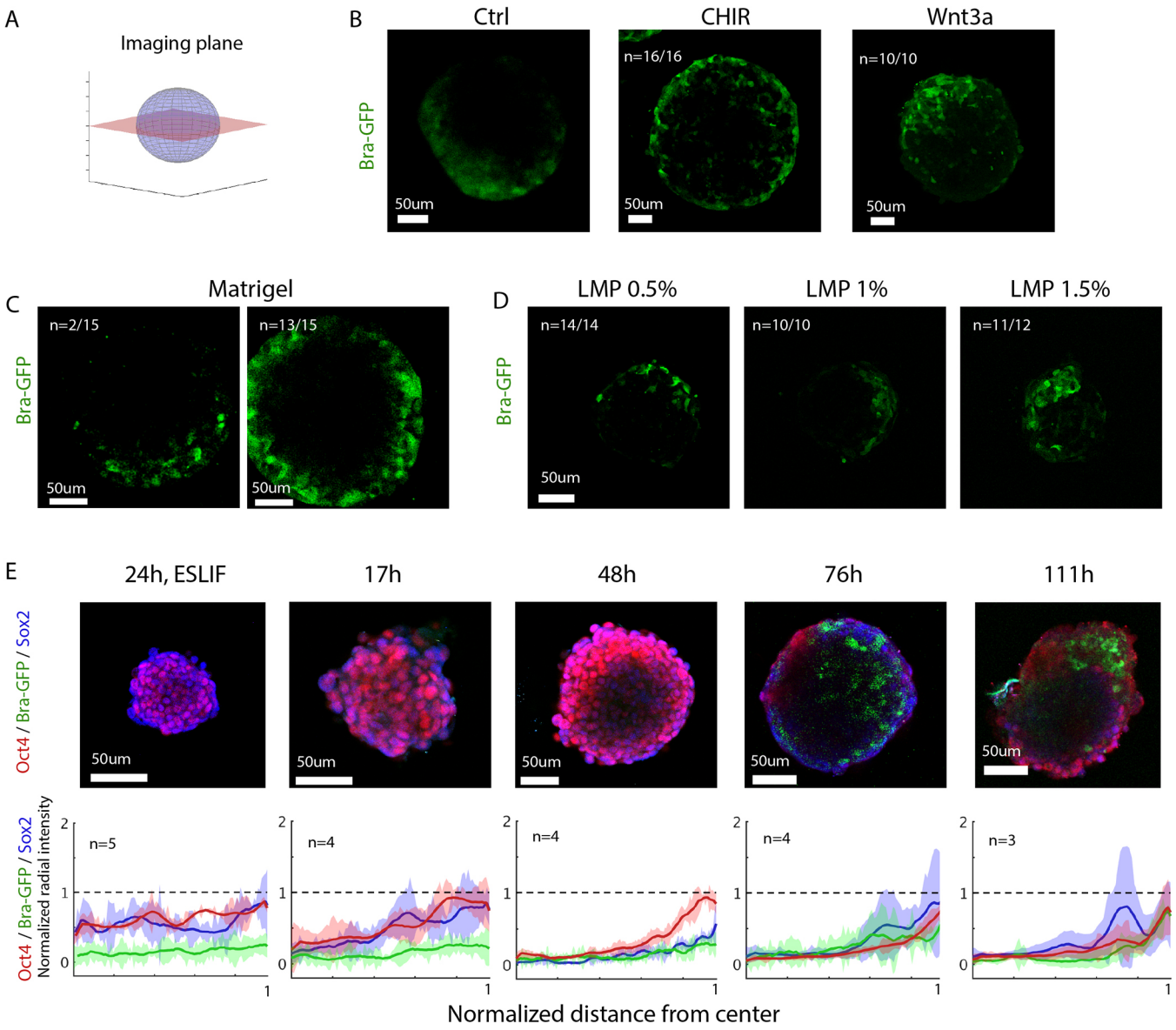

Fig. 2. A Bra-competent layer is formed prior to onset on the outer shell of the EB. (A) EBs are imaged at the equatorial slice. (B) Treatment with CHIR between 0–72 h (middle) triggers Bra onset on the entire shell, compared with control (left) or soluble Wnt3a treatment (right), which show a polarized onset. (C) Embedding EBs in Matrigel leads to Bra onset isotropically in most (13/15) EBs (right), or from a single locus in some (2/15) large EBs (left). (D) Embedding EBs in low melting point agarose (LMP) with various concentrations had no effect on Bra locus. (E) Immunostaining of Sox2 and Oct4 in E14 Bra-GFP EBs at the indicated time points after aggregation. Top row: equatorial slices. Bottom row: normalized radial intensity profiles of Oct4, Bra and Sox2, computed in the direction of maximal expression on the outer shell, averaged over the indicated number of EBs. Shaded area marks standard deviation.

in agarose generated a single locus onset, despite having isotropic contact with the gel (0.5%, n=14/14; 1%, n=10/10; 1.5%, n=11/12; Fig. 2D). Small EBs differentiated in microwells (mean EB radius at onset 78 µm, σ=10 µm, n=9) showed uniform isotropic onset (7/8 EBs, average onset time 78 h, σ=9 h), as also observed in small EBs embedded in Matrigel (Fig. S1D). This suggests that an isotropic pattern can be the result of size, which may be explained by a minimal locus size that is larger than the small EB surface or a minimal signal gradient requirement for a polarized pattern. In summary, a polarized Bra pattern can be obtained at contact points given sufficient EB size, but also under uniform gel contact, suggesting that this is a robust EB behavior. However, as demonstrated by results from CHIR induction, Wnt3a bead embedding and growth in Matrigel, the entire outer shell is competent to activate Bra, given strong activation of the Wnt pathway.

It has been suggested that Oct4 (Pou5f1) and Sox2 expression levels in differentiating ESCs direct their differentiation toward mesendoderm or neural ectoderm, respectively (Thomson et al., 2011). To test whether the competence of the outer shell can be explained by the expression pattern of these early pluripotency factors, we immunostained for Oct4 and Sox2 at 17, 48, 76 and 111 h after the start of differentiation. We observed that expression of both genes receded from the center toward the outer shell with time; by 72 h both Sox2 and Oct4 were highly expressed only at the outer shell of the EB (Fig. 2E).

Which molecular components mediate the effect of contact on Bra onset in outer layer cells? Fibronectin has been shown to induce Bra expression, and a mechanism linking fibronectin to Wnt signaling was proposed (Cheng et al., 2013). We therefore hypothesized that such a link can explain both the relation between contact and Wnt

Development (2019) 146, dev181917. doi:10.1242/dev.181917

signaling (leading to Bra onset) and the location choice for the Bra locus. We found that fibronectin was expressed isotropically on the outer shell of EBs, implying that its mere expression does not determine the location of Bra onset (Fig. 3A). We then inhibited fibronectin activity using an anti-Fn1 antibody, starting from 0, 24, 48 or 72 h after aggregation under differentiation conditions. Compared with the control group, which displayed normal Bra expression (16/16), fibronectin inhibition added at aggregation or at 24 h inhibited Bra expression (10/10 and 6/6 EBs, respectively, $P<2e{-}5$), had little to no effect when added at 72 h (4/4 EBs, $P<3e{-}4$) and a mixed effect when added at 48 h (8/8 EBs, $P<2e{-}6$) (Fig. 3B). Lack of Bra expression under fibronectin inhibition was also confirmed at the mRNA level (Fig. 3C). Our results suggest that the dependence of Bra-positive fate on fibronectin is limited to early stages, whereas the accumulation of Bra in cells and expansion of its expression to neighboring cells do not depend on fibronectin.

Wnt and contact signal sources are integrated to activate Bra

We found that both Wnt signaling and surface contact affect Bra expression onset, although our results suggest that contact bias is mediated through biochemical signaling. To further investigate how these two signal sources relate to each other in this context, we designed a system in which we can create a spatial separation between the surface contact point and a local source of Wnt signaling. To this end, we transfected HEK cells with a plasmid constitutively expressing either Wnt3a-P2A-H2B-CFP, Dkk1-P2A-H2B-Venus or, for the control group, H2B-CFP (Fig. 4A). A clump of HEK cells was then integrated into each EB at a random location shortly after aggregation. The EBs were then differentiated, as in the wild-type experiments, and the location of the Bra locus was analyzed with respect to the contact point and the locus of signaling cells using two-photon microscopy (Fig. 4B-D). In the EBs containing Dkk1 or Wnt3a cell clumps, the Bra locus overlapped with the plane defined by the EB centroid, HEKs and the contact point ($n=16$; average deviation from co-planarity 9.3°) (Fig. S2A). This allowed us to analyze the joint effects of contact and Wnt3a/Dkk1 signaling on Bra expression locus as angular deviations on a single plane (Fig. 4B). The amount of Wnt3a-secreting agents determined the effect on Bra locus bias from the contact. For small clumps of Wnt3a-expressing cells (3-5 cells), the source of Wnt3a led to a shift in the Bra locus, so that it was positioned between the contact point and the Wnt3a expressing locus (Fig. 4C,E-G). For larger clumps of Wnt3a-secreting cells (>10 cells), the Bra locus was pulled closer to the HEK cluster, maintaining a single locus ($P<0.05$ for all group pairs, two-sample KS-test; Fig. 4E,F). In one example, where the EB touched the microwell wall at the side opposite to the HEK clump, two Bra loci emerged, one next to the HEKs and one at the side contact point (Fig. S2B). In contrast, a source of Dkk1 shifted the Bra locus away from the contact point (Fig. 4D,E,G; $P<0.05$ for all group pairs, KS-test). This indicates that Dkk1 can exert its limiting effect over at least 150 µm.

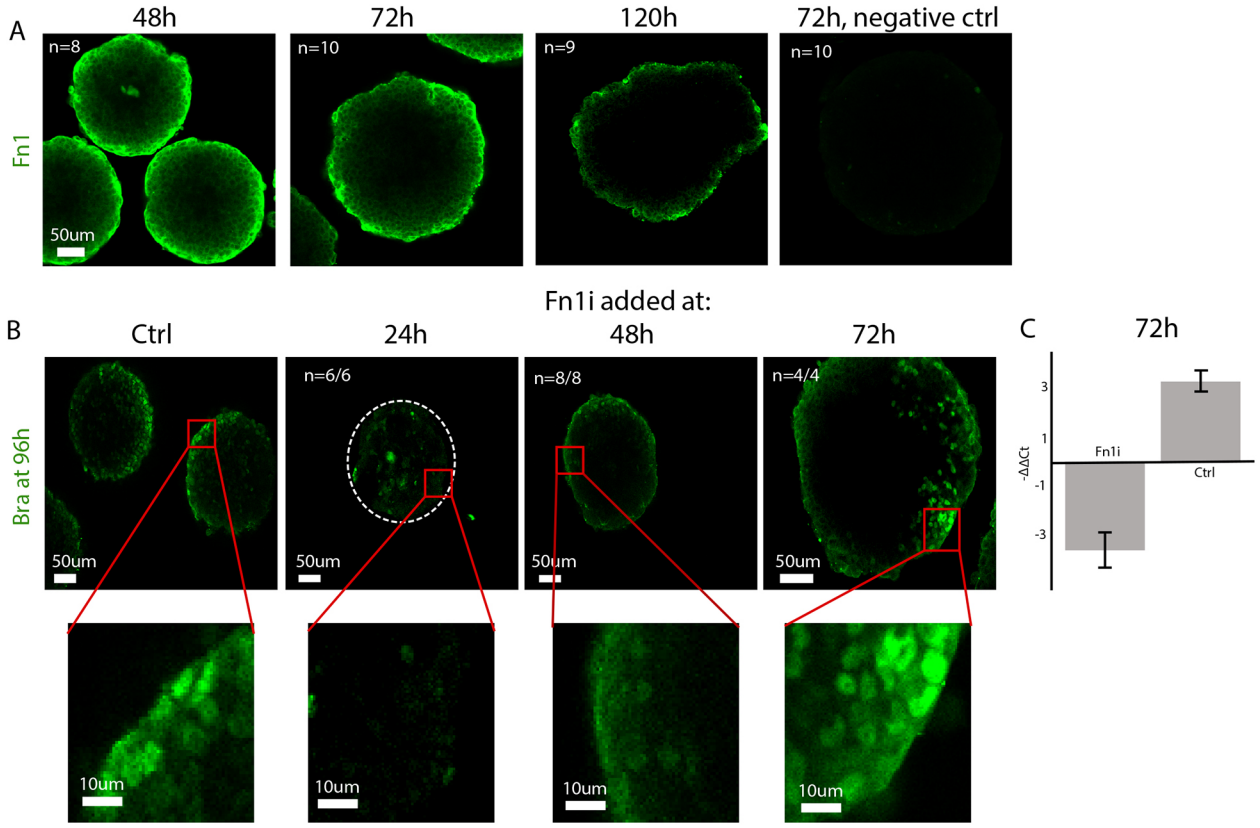

Fig. 3. Fibronectin is expressed isotropically on the EB outer shell, and is needed at early stages for Bra expression. (A) Fibronectin immunostaining at 48, 72 and 120 h from aggregation in R1-derived EBs. Fibronectin is expressed uniformly on the outer shell at early stages, but declines by 120 h. Negative control (right) shows secondary-only staining. The example for each condition is representative of all imaged EBs. (B) EBs subjected to fibronectin inhibition by an anti-Fn1 antibody (Fn1i) starting at 24, 48 or 72 h from aggregation, and immunostained for Bra (green) at 96 h (close to the onset time in R1-derived EBs). Fibronectin inhibition prevents Bra onset, but only when started earlier than 48 h. (C) Bra levels measured by RT-PCR, showing Bra expression fold change between control group (no treatment) and Fn1i treatment group. Fn1i was added at aggregation. Mean±s.d. for three primer pairs and two replicates each are shown ($P<1e{-}4$; see Materials and Methods).

Development (2019) 146, dev181917. doi:10.1242/dev.181917

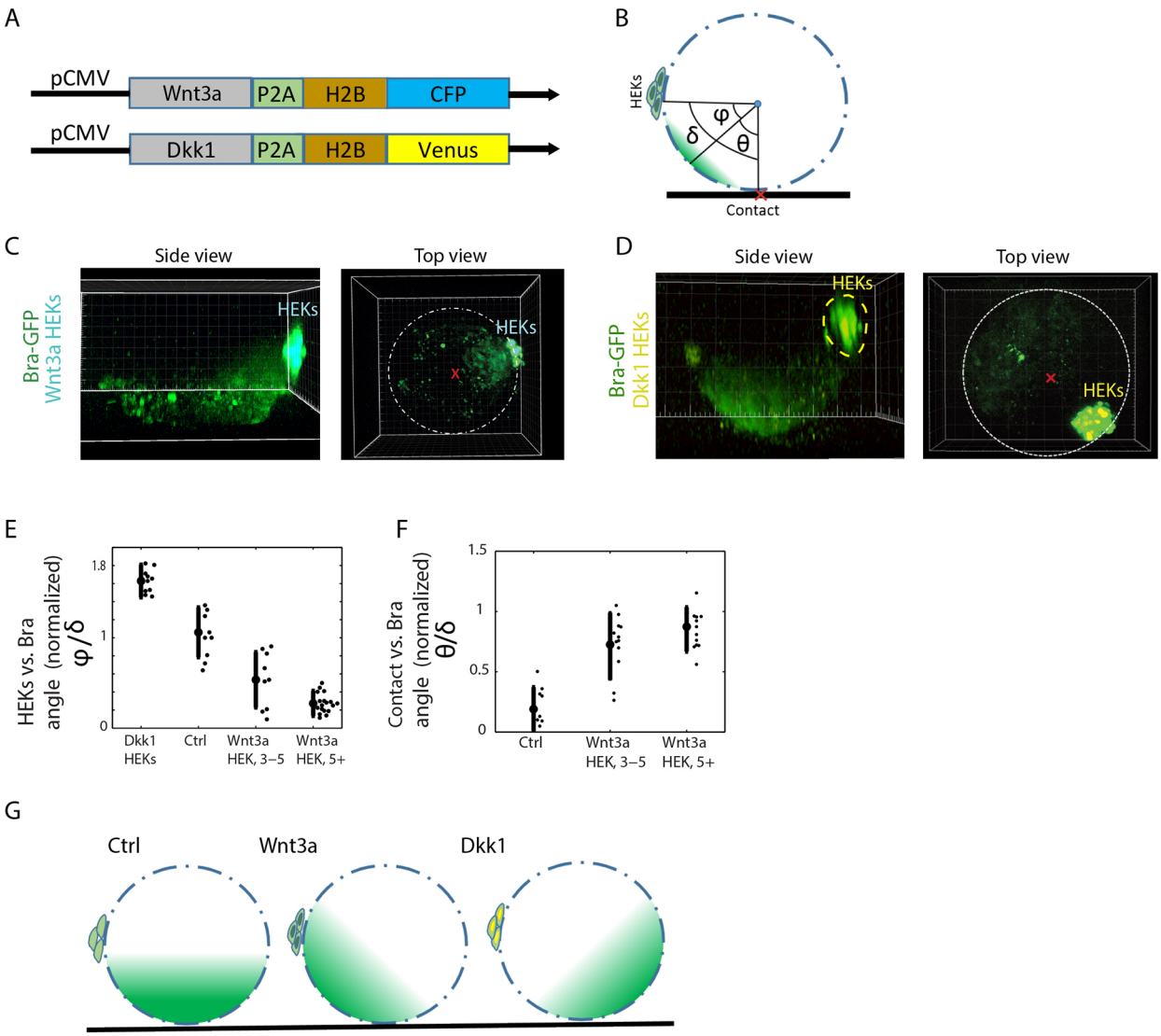

Fig. 4. Bra onset locus is determined by contact and Wnt signaling integration. (A) Wnt3a and Dkk1 constructs used for ligand secretion from HEK cells. (B) A signal source (a clump of transfected HEK cells) was embedded into each EB. After 72 h of differentiation, the position of the signal source and the Bra locus were determined, as in Fig. 1D. The pairwise spatial angles between signal source, contact point with well bottom surface (red cross) and Bra locus were then computed. (C) Example of an EB with a Wnt3a signaling source. Bra onset locus is biased toward the Wnt3a-secreting HEKs. (D) Example of an EB with a Dkk1 signaling source. Bra onset locus is biased away from the Dkk1-secreting HEKs. (E) Angle between HEK signaling source and Bra locus (ϕ) normalized by the angle between the HEKs and the contact point (δ). Wnt3a secretion biases onset from the contact point toward the Wnt source in a quantity-dependent manner, whereas Dkk1 secretion biases the locus away to the opposite side. $P<0.05$ for all group pairs, two-sample KS test. (F) Angle between contact point and Bra locus (θ) normalized by the angle between the HEKs and the contact point (δ). (G) Scheme of the spatial bias effect.

Moreover, the locus shift from the contact point, toward or away from the signaling source shows how Wnt3a and Dkk1 signal integration determines the locus location. In control EBs (harboring clumps of H2B-CFP cells) we saw no spatial effect on the locus of Bra onset, which was mostly at the contact point (Fig. 4E,F). These results suggest that contact and Wnt effects on Bra onset are integrated rather than override each other. One possible explanation is that contact mediates Wnt signaling (which is then spatially summed with the other source of Wnt signal). It is also possible, however, that contact acts through a different signaling pathway, which is summed with the Wnt pathway in triggering Bra onset.

Foxa2 is a precursor to symmetry breaking and Bra onset locus

To explain the choice of Bra onset location in the absence of external contact surfaces (i.e. in hanging drops), we examined additional genes that are predicted to be expressed at or near the primitive streak before gastrulation. We have previously suggested that once Bra expression begins, the EB progresses at a common developmental pace, delineating a differentiation plan associated with multiple early development genes (Boxman et al., 2016). We therefore hypothesized that the spatial expression pattern of key proteins in EBs before and during Bra onset shows similarity to their *in utero* pattern around the primitive streak. To test this, we immunostained EBs differentiated in hanging drops for a few early markers at different time points from aggregation, and checked how their spatial expression patterns related to that of Bra. We found that Eomes, a primitive streak marker regulated by Nodal and an EMT driver, was localized to the same pole as Bra although it expanded further on the outer shell (Fig. 5A). E-cadherin (Cdh1) was expressed throughout the EB prior to Bra expression onset, but then its expression declined

Development (2019) 146, dev181917. doi:10.1242/dev.181917

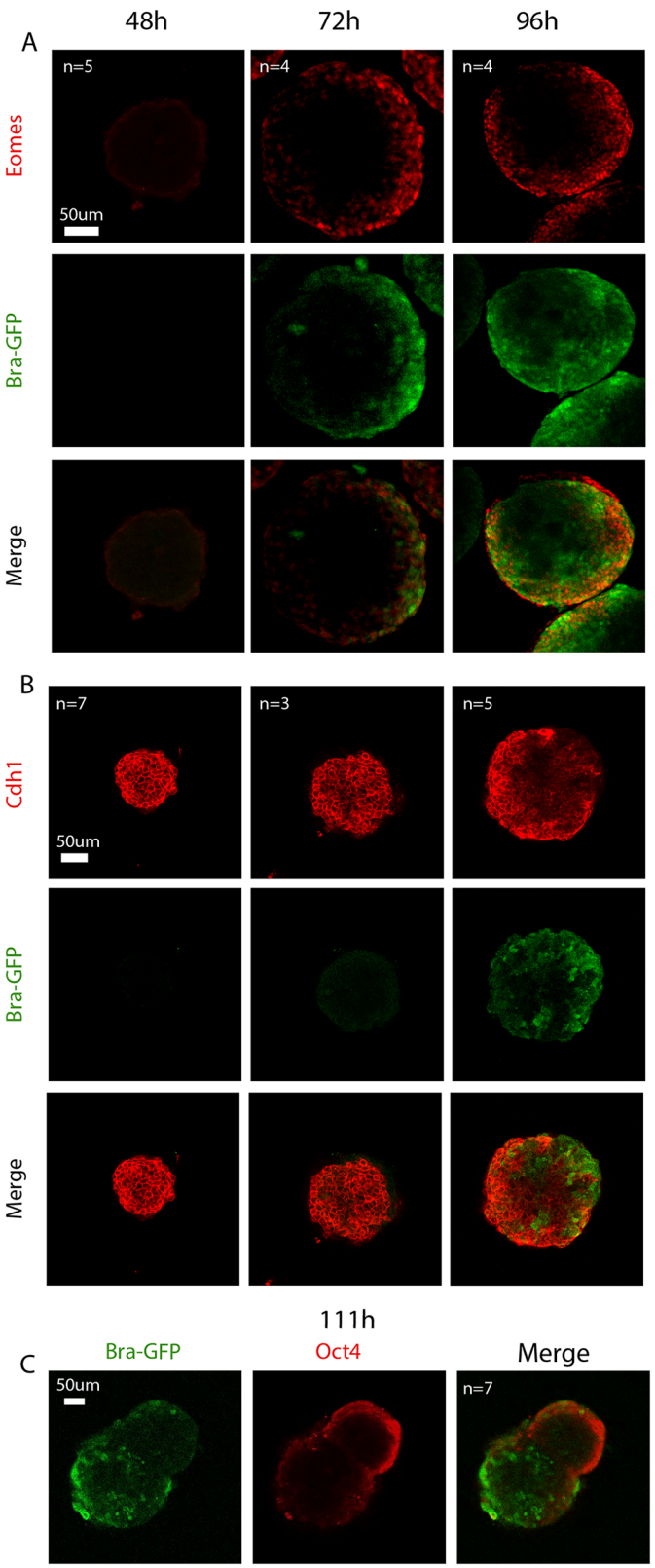

Fig. 5. Bra onsets in a primitive streak like area in EBs. Immunostaining of early developmental markers, comparing their spatial expression patterns to that of Bra. (A) Eomes onsets with Bra at the same locus and extends beyond Bra spatial expression. (B) E-cadherin recedes from the locus where Bra appears, allowing cell motility. (C) Oct4 is expressed on the outer shell, then recedes to the pole opposite that of Bra onset. The example shown for each condition is representative of all imaged EBs under that condition.

where Bra was expressed, indicating that epithelial mesenchymal transition takes place in the EB (Fig. 5B) (ten Berge et al., 2008). Loss of E-cadherin enables cell movement, which is supportive of previous observations of gastrulation-like events in EBs and 2D models (Boxman et al., 2016; van den Brink et al., 2014; Warmflash et al., 2014) and is consistent with primitive streak behavior. Oct4, whose expression initially declines in the inner layers, gradually receded on the outer shell toward the opposite pole as Bra expression expanded, similar to the opposing gradients observed in late streak stage epiblasts (Figs 2E and 5C).

These examples demonstrate how the expression and spatial arrangement of different proteins in the EB during pre-streak and through streak phases resemble the equivalent *in vivo* stages, albeit with an altered topology. Because the primitive streak is initiated adjacent to the visceral endoderm layer in the embryo, we tested for spatiotemporal correlation of the visceral endoderm marker Foxa2 with Bra in the EB. Such a correlation could point to an additional driving factor in Bra locus determination. Foxa2 expression appeared up to 24 h prior to Bra at an internal area within the EBs, with Bra onset following on the shell juxtaposed to Foxa2-expressing cells (Fig. 6A), suggesting a common driver or interlayer dependency. This spatial relation between Foxa2 and Bra was accentuated in large EBs (~700 µM in diameter at onset) (Fig. 6A, bottom; Fig. S3A), suggesting that these two cell populations have a regulatory relation. To better characterize Foxa2 cells around their onset, we examined the expression of Gata6 and Sox17 at 48 h. Sox17 was not expressed at this early time point. Similarly, no Gata6 expression was detected in the EBs (Fig. S4D), consistent with previous reports (Turner et al., 2017; van den Brink et al., 2014). This indicates that Foxa2-positive cells at this stage do not represent primitive endoderm or visceral endoderm, but probably posterior epiblast or early anterior streak identities (Arnold et al., 2000; Burtscher and Lickert, 2009; Cai et al., 2008; Choi et al., 2012).

To look for candidate genes that could convey the regulation of Bra next to Foxa2-positive cells, we analyzed a published single-cell expression dataset from E6.5 mouse embryos (Scialdone et al., 2016). We found that within epiblast cells, both Foxa2-expressing cells and Bra-expressing cells were significantly enriched for porcupine (Porcn) expression (P=2.6e–8 and P=8.83e–10, respectively). Porcn palmitoylation of Wnt ligands is required for their secretion, suggesting that Foxa2-positive cells in EBs secrete Wnt ligands to the adjacent perimeter, thus promoting the onset of Bra in an adjacent locus. We therefore immunostained for Porcn in differentiating EBs and found that Porcn expression was spatially limited to areas adjacent to and overlapping the Bra onset locus (Fig. 6B). Inhibiting Porcn activity with IWP-2 starting either at aggregation or 48 h after aggregation (when Foxa2 is already expressed in the volume) resulted in the abolishment of both Bra and Foxa2 (Fig. 6C; Fig. S4A). A similar result was obtained by selectively activating non-canonical Wnt with Wnt5a; however, blocking canonical Wnt using XAV-939 or Wnt secretion using IWP-2 resulted in no expression of Bra or Foxa2. Adding just Wnt5a had no significant effect on expression of Bra and Foxa2 compared with the control group (XAV-939+Wnt5a, 0/10, P=1.2e–4; IWP-2+Wnt5a, 0/10, P=1.2e–4; Wnt5a, 8/8; control, 6/6; Fig. S4C). This suggests that both genes require canonical Wnt signaling for their expression (Gadue et al., 2006; Sawada et al., 2005). We were able to rescue Bra by introducing IWP-2 with CHIR to the EBs at 48 h after aggregation; however, Foxa2 was fully downregulated. When Wnt3a was added to IWP-2, we obtained a partial rescue of both Bra and Foxa2. Interestingly, perturbing the EBs with just CHIR or Wnt3a gave a similar result; Bra was

Development (2019) 146, dev181917. doi:10.1242/dev.181917

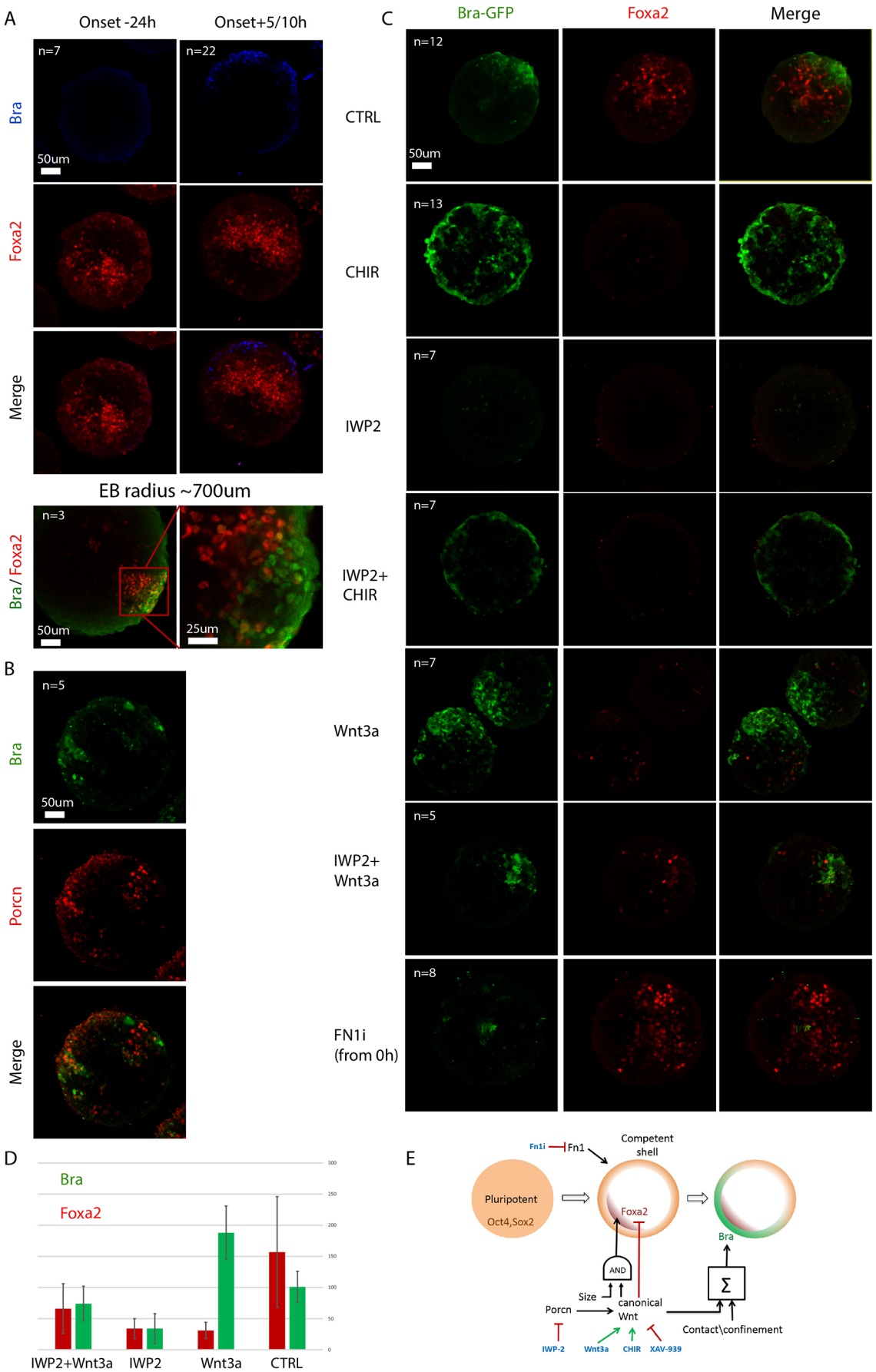

Fig. 6. See next page for legend.

Development (2019) 146, dev181917. doi:10.1242/dev.181917

Fig. 6. Foxa2 is a Wnt dependent precursor to symmetry breaking and Bra expression locus. (A) Foxa2 expression is juxtaposed to Bra-positive cells in EBs, appearing >24 h before the onset of Bra (*n*>20, multiple experiments). Bottom: Foxa2/Bra pattern in a large (700 µm) EB (similar pattern seen in 3/3 large EBs). (B) Porcn expression partially overlaps with Bra, suggesting that Wnt ligands can be secreted in these cells. (C) CHIR upregulates Bra, triggers an isotropic expression pattern on the Bra-competent outer shell while downregulating Foxa2 expression in the EB; IWP2 (a porcupine inhibitor) inhibits Wnt secretion, downregulating Foxa2 and Bra; CHIR rescues Bra under IWP2 perturbation, but Foxa2 is still downregulated; Wnt3a upregulates Bra while downregulating Foxa2; Wnt3a partially rescues both Bra and Foxa2 under IWP2; fibronectin inhibition abolishes Bra expression but leaves Foxa2 intact. All signals were applied from 48 h after aggregation, except fibronectin inhibition, which was applied at 0 h. Patterns are representative for all imaged EBs in each condition. (D) Perturbation effects on Bra and Foxa2 expression quantified as number of highly expressing cells per EB. (E) Scheme summarizing the factors affecting Foxa2 and Bra onset in the EB.

over-expressed and Foxa2 was either fully (in the case of CHIR) or partially downregulated and spatially decoupled from Bra (in the case of Wnt3a) (Fig. 6C,D; Fig. S3B). These results suggest that an intricate, probably dynamic, signaling balance involving canonical Wnt determines and maintains the fate of these cells. In small EBs (<65 µm radius) Foxa2 had small to negligible expression whereas Bra encompassed the entire EB (5/5; Fig. S4B). This suggests that the EB requires a certain volume (or length scale) to allow the development of two distinct cell populations, consistent with results in 2D colonies (Morgani et al., 2018; Warmflash et al., 2014). The threshold size might be required to establish sufficient differences, or gradients, in signaling activity. Furthermore, although Bra expression was abolished under fibronectin inhibition starting at aggregation, Foxa2 showed wild-type expression, pointing to a fate decision made at least 24 h before Bra onset and leading to Foxa2-positive cells (Fig. 6C, bottom).

Together, these results show how Bra and Foxa2 are spatially related under canonical Wnt signaling. Bra is monotonically upregulated by canonical Wnt whereas Foxa2 shows a more complex regulation nature, being upregulated by an intermediate level of canonical Wnt activation but downregulated by a strong level (Fig. 6E).

DISCUSSION

Here we dissect the factors and mechanisms affecting the polarized expression pattern of Bra expression in EBs. These patterns can be formed in EBs and gastruloids with no extra-embryonic tissue and no external Nodal or BMP sources (Boxman et al., 2016; Turner et al., 2017; van den Brink et al., 2014). We have shown that physical contact with surfaces, a localized source of Wnt signaling and proximity to Foxa2-expressing cells can all induce or predict the onset of Bra. Interestingly, in the embryo, these three conditions co-occur near the future location of the primitive streak, making it hard to dissect their respective roles. Bra expression begins during gastrulation near a source of Wnt signaling (arising from a positive feedback loop between Bmp4 sourced from the ExE and Nodal and Wnt at the posterior epiblast), adjacent to Foxa2-positive cells, in a region that might have experienced high mechanical pressure as a result of implantation. We analyzed some of the hierarchy between these three primitive streak predictors (Fig. 6E).

Bra onset polarization was robust to different external conditions and EB parameters, suggesting that it is the ‘default’ behavior in this system. A similar result was demonstrated in mouse embryos grown *in vitro*, where mechanical contact might direct AP axis formation and positioning of the AVE, but they can also robustly form in hanging drops (Bedzhov et al., 2015; Hiramatsu et al., 2013). The polar pattern in EBs can be obtained even in the absence of any chemical or physical cue directing its orientation (as seen in the agarose embedding experiments). Overriding this polarization process pattern in EBs required specific intervention, such as continuous canonical Wnt activation by CHIR or application of inducing sources (contact points or localized Wnt sources) at two distant locations on the EB surface (Fig. 1G; Fig. S2B). Contact with external surfaces, or with the hanging drop boundary surface, was sufficient to bias the location of Bra onset and orient the EB primary axis. We have shown how we can generate two Bra loci through controlled contact, depending on the geometry of the surrounding surfaces. The fact that the onset of Bra expression in hanging drops or large wells was similar to that in narrow micropools suggests that it is not the effect of mechanical pressure, but of the interface with contact surface or of geometrical confinement. These could act through limiting the diffusion of secreted signal molecules, such as Wnt ligands, resulting in locally higher signal concentration (Siggia and Warmflash, 2018). Another option is that the ligand activation mechanism is bypassed through interfacing with outside surfaces by integrin-mediated signaling (Cheng et al., 2013) or by mechanotransduced phosphorylation of β-catenin (Brunet et al., 2013), although the localization of the Bra locus in hanging drops to the bottom air–liquid interface suggests that diffusion confinement is sufficient. Interestingly, the factors that we found to affect the Bra locus in 3D were very different from those in the case of 2D patterned colonies, where a recent study related the percentage of Bra-positive cells to cell density, and their localization to high curvature regions at the tip of elongated colonies (Blin et al., 2018). In 2D colonies, there is no equivalent for limited ligand diffusion in 3D near surfaces, and alternative factors might bias the response potential in different locations within the colony (Etoc et al., 2016).

We found that the potential to initiate Bra expression was limited to cells at the outer layers of the EB, at least in large-enough EBs, and its expression did not expand much inwards. Whole-volume Bra expression was observed mostly in small EBs. The patterns of Sox2 and Oct4 expression suggest there could be multiple expression and epigenetic differences between different EB layers prior to Bra onset, which could explain the biased expansion pattern, despite positive feedback between Bra and Wnt signaling (Evans et al., 2012; Yamaguchi et al., 1999). The limitation of Foxa2 initiation to inner EB cells provides further support for the differential potentials in different EB layers.

We found that we can ‘pull’ or ‘push’ the Bra locus away from the contact point by using an external source of Wnt3a- or Dkk1-secreting cells, respectively. This demonstrates that contact and biochemical signal modalities can be summed by the EB, resulting in a single locus, as opposed to the two loci or one locus overriding the other that we observed in the forced contact experiments. This can be attributed to the gradient strength or to the surface distance between the loci, which might be too large for signal integration to have an effect. One possible mechanism for this integration is activation of Wnt signaling through mechanical contact. The dependence of Bra activation on fibronectin points to such a mechanism (Cheng et al., 2013). Interestingly, the mechanism proposed by Cheng et al. (2013) bypasses the Wnt pathway receptors and therefore cannot explain why Dkk1 diverts Bra onset away from the contact point, suggesting other mechanisms are at play. Another option is that Wnt ligands consolidate at the contact surfaces, or have limited diffusion range near them, leading to locally higher concentration (Siggia and Warmflash, 2018). This option is particularly reinforced by localization of the Bra locus to the air–water interface in hanging drops, where we do not expect to find integrin interactions. The

Development (2019) 146, dev181917. doi:10.1242/dev.181917

isotropic peripheral onset we observed in small EBs could be attributed to a lack of Wnt gradient formation.

The relation of Bra onset to Foxa2-positive cells provides some interesting insights. First, from the differential response to fibronectin inhibition, we conclude that the decision junction of differentiating ESCs within the EB toward Bra and Foxa2 tissue layers takes place at 24-48 h prior to Bra onset. The lack of overlap with visceral or definitive endoderm markers suggests that Foxa2-positive cells initially represent a non-endodermal population, such as anterior primitive streak (Burtscher and Lickert, 2009; Gadue et al., 2006). Second, the observation that small EBs do not express Foxa2 suggests that a signal gradient controls segregation between these two cell populations, which potentially represent posterior and anterior primitive streak. This is reinforced by the dependency of Foxa2 expression on intermediate canonical Wnt signaling, as well as by the high spatial dependency seen between these two cell populations in large EBs (Fig. 6; Fig. S3). The facts that different perturbations can lead to Bra or Foxa2 expression while abolishing the other fate in the EB and that the spatial adjacency of these two cell populations can be decoupled using external Wnt signaling suggest that the observed spatial relation is a result of the dependence of both proteins on different levels of canonical Wnt signaling, which can be spatially coupled through a morphogen gradient. The earlier onset of Foxa2 relative to Bra might be because Foxa2-competent cells, which form within the inner EB layers, require lower levels of canonical Wnt (which can be reached earlier), whereas Bra requires higher levels of canonical Wnt. Another option is that the Foxa2 locus (or its relevant enhancer) becomes accessible earlier than that of Bra. Further molecular work is needed to decipher the Foxa2 onset mechanisms.

In contrast to its location, the timing of Bra expression onset in EBs was not affected by external or localized Wnt3a signaling, or by inducing early contact in narrow microwells. These results point to the maturation needed in outer shell cells before they become Wnt- and/or contact-responsive to induce Bra. Further characterization of the chromatin or expression changes defining that ‘mature’ state are needed.

Through different perturbations on a 3D *in vitro* system we were able to delineate the basic dependencies of an early fate decision on contact and biochemical factors that co-occur in the embryo. The insights we gained here improve our understanding on the forces shaping differentiation within *in vitro* systems such as EBs and gastruloids and shed more light on how they are integrated *in vivo*.

MATERIALS AND METHODS

Cell culture

E14 Bra-GFP mESCs (kindly provided by Dr Gordon Keller, McEwen Stem Cell Institute, UHN, Toronto, Canada), R1 mESCs and SuTOP-CFP, AR8-RFP mESCs (kindly provided by Dr Palle Serup, University of Copenhagen, Denmark) were cultured using standard conditions on irradiated primary mouse embryonic fibroblasts and knockout DMEM containing 15% fetal bovine serum, 50 µg/ml penicillin/streptomycin, 2 mM L-glutamine, 100 µM nonessential amino acids, 80 µM β-mercaptoethanol and 10^3 U/ml LIF.

EB formation and differentiation

Embryoid bodies were formed in hanging drops under differentiation conditions. Each drop contained 25 µl differentiation medium (IMEM containing 20% FBS, 50 µg/ml penicillin/streptomycin, 2 mM L-glutamine, 100 µM nonessential amino acids, 100 µM β-mercaptoethanol) with approximately 300 mESCs; 100 cells for small EB experiments, 2000 cells for large EB experiments. The number of cells in hanging drops was controlled using a cell counting slide and dilution of the cell-containing medium to obtain the desired starting cell number per single EB within each 25 µl hanging drop. Cells were aggregated for 24 or 48 h before being transferred to micropools or microwells for imaging in the same medium. Alternatively, the EBs were kept in hanging drops for the entire duration of the experiment before being imaged or fixed and immunostained. In some of the staining experiments (Figs 3 and 6A; Fig. S3), R1-derived EBs were used. In these EBs, Bra onset typically occurs about 12 h later than in E14-derived EBs. When adding inhibitors or activators to hanging drops, we aggregated the EBs in 20 µl hanging drops and then added at the appropriate time 5 µl of medium with the required substance. For signal perturbation experiments, differentiation medium was supplemented with CHIR99021 (5.35 µM) or recombinant Wnt3a (500 ng/ml). For fibronectin inhibition, the medium was supplemented with anti-Fn1 antibody (Abcam, ab6328). To incorporate Wnt3a-bound beads within the EB, prepared beads (kindly provided by Shukry J. Habib, King's College London, UK) were premixed with mESCs before distributing the suspension to 25 µl hanging drops for aggregation. We added 12,000 beads to 10 ml of medium with the mESCs, averaging 30 beads per EB. Bead integration into the EBs was confirmed by two-photon microscopy (Fig. S1B).

Hydrogel and matrigel

Low melting point agarose (Sigma-Aldrich, A9414) was mixed with preheated double-distilled water and vortexed to avoid clumps. It was then deposited on the glass bottom of a 24-well plate to allow two-photon imaging. EBs were injected into the gel when it had cooled down sufficiently, about 24 h after aggregation in hanging drops. Matrigel (Gibco Geltrex, A1413202) was thawed on ice in 4°C overnight. Matrigel drops (20 µl each) were deposited on the glass bottom of a 24-well plate. EBs were transferred into the drops at 48 h after aggregation; after gel solidification, the wells were filled with differentiation medium.

HEK incorporation in EBs

HEK 293 cells were split to three wells (12-well plate, 50% confluence). After 12 h, the cells were transfected with constitutive pCMV-H2B-Cerulean, pCMV-Wnt3A-P2A-H2B-Cerulean or pCMV-DKK1-P2A-H2BVenus plasmids, using the Xfect transfection reagent (631318). At 24 h post transfection, the transfected HEKs were trypsinized, suspended as single cells and injected into hanging drops containing 12-h-old E14 Bra-GFP EBs at different concentrations (10, 20 or 50 HEKs per EB). After 24 h, the injected EBs were transferred into microwells and imaged using a two-photon microscope.

Micropool patterning with deep reactive-ion etching and microwells

To create the silicon template for the shaped micropools and microwells, we implemented a high aspect ratio etching system usually used for microelectronics fabrication. Using deep reactive-ion etching (DRIE), we were able to determine the micropattern’s exact depth by selecting a wafer with a specific handle/device thickness. This suggests an advantage over the common photoresist techniques, which require fine-tuning of the process to obtain an exact pattern depth. We fabricated 200-500 µm diameter microwells and 100-500 µm wide micropools, with a depth of approximately 400 µm. The patterns were then coated with PTFE to minimize friction with the template when pulling the elastomer out. To create the microwell/pool negative, PDMS elastomer (Sylgard 184) mixed with a curing agent (1:10) was poured into the silicon wafer mold and incubated overnight at 50°C. Individual stamps were then cut out using a scalpel. To generate the positive agar microwells/pools we placed the stamps face down inside glass-bottom plates coated with poly-D-lysine and injected agarose under the stamps. The plates with the injected stamps were then placed in a vacuum chamber for 90 min, followed by another round of agar injection and an additional 10 min in the vacuum chamber. The stamps were then removed, leaving the micropatterns imprinted in the agar.

Imaging of hanging drops

EBs were aggregated in hanging drops on plastics slides. The slides were mounted in the two-photon microscope and imaged with EC Plan-Neofluar 20×/0.50 dry objective, providing a working distance of 2 mm. The data were then segmented in Imaris and analyzed in MATLAB.

Development (2019) 146, dev181917. doi:10.1242/dev.181917

Live imaging

We sourced data from both 2D and 3D live imaging experiments. 2D epifluorescence experiments offer a short acquisition cycle for a large cohort of EBs, thus yielding accurate temporal tracking and statistics based on a large number of samples. On the other hand, they do not possess elevation distinction and the superior resolution and cell separation that more advanced microscopy techniques offer. For 3D imaging, we used a two-photon microscope with which we were able to have a full view of signal dynamics and track individual cells. However, this technique requires large data analysis, has a longer acquisition cycle and is less compatible with multiple EB imaging. Two-photon imaging was carried out using a Zeiss LSM7 inverted two-photon microscope with a Plan-Apochromat 20×/0.8 dry objective. Each EB was scanned at 3 µm intervals along the *z*-direction. Horizontal resolution was set to 512×512 pixels at approximately 0.6 µm per pixel, 8 bit depth. GFP was excited at 930 nm. RFP, Alexa Fluor 488, 405 and 594 were excited at 800 nm. CFP was excited at 860 nm. Epifluorescence imaging was carried out using a Nikon TiE epifluorescence microscope equipped with a motorized XY stage (Prior) at 10× magnification using NIS Elements software. Acquisitions were taken every 25 or 30 min for 14–72 h. For live imaging, in both systems we used Okolab incubation cages, maintaining 5% CO_2 and 37°C.

Real-time PCR

Three different primer pairs were designed for different Bra exons, and two for each of the housekeeping genes *Ywhaz* and *Rock2*. EBs were gathered from different pools, distinct from each other by experiment group. mRNA was extracted by disassembling by pipetting and incubating the pooled EBs for 5 min in 0.5 ml Trizol (Sigma-Aldrich T9424-25 ml), followed by adding 100 µl chloroform and another 5 min incubation. After centrifuging the samples for 10 min at 12,000 ***g*** at 2-8°C, the translucent phase was incubated in IPA 100% for 10 min at room temperature. Centrifuging the samples again in the same manner gave a pellet containing the mRNA, to which we added 100 µl 70% ethanol, vortexed the samples and then centrifuged the samples for 5 min at 10,000 ***g*** at 2-8°C. The ethanol was then removed and the rest vaporized within 15 min, followed by addition of double-distilled water. We then produced cDNA (Invitrogen, 18080-051) and performed RT-PCR (Thermo Fisher StepOnePlus Real-Time PCR system) using Fast SYBR Green (Thermo Fisher, 4385612). Each Bra primer pair was run in duplicate. Results were normalized by subtracting the average result for housekeeping genes (ΔCt) and then subtracting the control group (−ΔΔCt).

Immunofluorescence

We fixed the embryoid bodies with 4% paraformaldehyde overnight at 4°C, followed by a rinse cycle and an overnight wash in PBS. We added primary antibodies against Eomes (Abcam, ab23345), Bra (R&D Systems, AF2085), Foxa2 (Abcam, ab108422-100), E-cadherin (Cell Signaling, 24E10), Oct4 (Santa Cruz Biotechnology, sc-8628) and Sox2 (Santa Cruz Biotechnology, sc-365964) with blocking buffer (PBS, 0.1% Triton X-100, 5% FBS) and incubated overnight at 4°C, followed by four wash cycles in blocking buffer for at least 30 min per cycle. We then added Alexa Fluor-conjugated secondary antibody in blocking buffer and incubated it overnight, followed by four wash cycles as described for the primary antibody. Antibody concentrations used were the same as recommended by the manufacturer for 2D staining.

Segmentation and analysis

The two-photon microscopy data were contrast enhanced in Fiji and then spot segmented in Imaris, where the integration radius was set to 7 µm and the filter was set to sum intensity with a threshold of 110/255. The background was subtracted prior to segmentation. The segmented data were read and analyzed in MATLAB. For Bra locus estimation in hanging drops or microwell experiments, locus elevation and azimuth angles were calculated from the segmented two-photon data by the sum vector of all Bra-positive cells. Bra onset was defined as 'polarized' when Bra-GFP occupied less than 25% of the shell, in one locus. The EB center and radius were estimated by Bra-positive cell curvature. The angle between the EB bottom point and Bra locus was then computed. For HEK incorporation experiments, we developed a MATLAB script that calculates geometrical properties between the HEK cluster, Bra locus and contact point. The script detects HEK cells at each time point by channel and intensity. We calculated the geometrical mean of the HEKs and set it as the HEK location point. Next we looked for the Bra locus, where a locus is defined as a minimum of five cells above the intensity threshold of 100 within a distance of 50 µm from each other, all in the green channel. Next, we defined the contact point of the EB with the well bottom as the bottom point of the sphere and calculated the geometric properties between all pairwise combinations of HEK cluster, Bra locus and contact point. The geometrical properties calculated were the spatial angles, Euclidean distances and geodesic distances. Side onset in microwells was manually detected by superimposing the GFP signal on brightfield images in which both the EB and the microwell wall are clearly visible, as shown in Fig. 1. Angle quantification was automatically performed using a MATLAB script on 3D segmented data.

Acknowledgements

We thank Shukri Habib for providing Wnt3a-coated beads, Palle Serup for the SuTOP-CFP mESC line, Amitai Menuchin for help with RT-PCR, and David Sprinzak, Omri Wurzel and the three anonymous reviewers for providing helpful feedback on the manuscript.

Competing interests

The authors declare no competing or financial interests.

Author contributions

Conceptualization: N.S., I.N.; Methodology: N.S., S.S., M.A., M.P., J.B., I.N.; Software: N.S.; Validation: I.N.; Formal analysis: N.S., S.S.; Investigation: N.S., S.S., M.A., M.P., G.S., J.B.; Writing - original draft: N.S., I.N.; Writing - review & editing: N.S., I.N.; Supervision: I.N.

Funding

This study was supported by the Israel Science Foundation (1665/16) and by a fellowship from the Edmond J. Safra Center for Bioinformatics at Tel-Aviv University.

Supplementary information

Supplementary information available online at
http://dev.biologists.org/lookup/doi/10.1242/dev.181917.supplemental

References

Arnold, S. J. and Robertson, E. J. (2009). Making a commitment: cell lineage allocation and axis patterning in the early mouse embryo. *Nat. Rev. Mol. Cell Biol.* **10**, 91-103. doi:10.1038/nrm2618

Arnold, S. J., Stappert, J., Bauer, A., Kispert, A., Herrmann, B. G. and Kemler, R. (2000). Brachyury is a target gene of the Wnt/beta-catenin signaling pathway. *Mech. Dev.* **91**, 249-258. doi:10.1016/S0925-4773(99)00309-3

Beccari, L., Moris, N., Girgin, M., Turner, D. A., Baillie-Johnson, P., Cossy, A.-C., Lutolf, M. P., Duboule, D. and Arias, A. M. (2018). Multi-axial self-organization properties of mouse embryonic stem cells into gastruloids. *Nature* **562**, 272-276. doi:10.1038/s41586-018-0578-0

Bedzhov, I., Bialecka, M., Zielinska, A., Kosalka, J., Antonica, F., Thompson, A. J., Franze, K. and Zernicka-Goetz, M. (2015). Development of the anterior-posterior axis is a self-organizing process in the absence of maternal cues in the mouse embryo. *Cell Res.* **25**, 1368-1371. doi:10.1038/cr.2015.104

Blin, G., Wisniewski, D., Picart, C., Thery, M., Puceat, M. and Lowell, S. (2018). Geometrical confinement controls the asymmetric patterning of brachyury in cultures of pluripotent cells. *Development* **145**, dev166025. doi:10.1242/dev.166025

Boxman, J., Sagy, N., Achanta, S., Vadigepalli, R. and Nachman, I. (2016). Integrated live imaging and molecular profiling of embryoid bodies reveals a synchronized progression of early differentiation. *Sci. Rep.* **6**, 31623. doi:10.1038/srep31623

Brunet, T., Bouclet, A., Ahmadi, P., Mitrossilis, D., Driquez, B., Brunet, A.-C., Henry, L., Serman, F., Béalle, G., Ménager, C. et al. (2013). Evolutionary conservation of early mesoderm specification by mechanotransduction in Bilateria. *Nat. Commun.* **4**, 2821. doi:10.1038/ncomms3821

Burtscher, I. and Lickert, H. (2009). Foxa2 regulates polarity and epithelialization in the endoderm germ layer of the mouse embryo. *Development* **136**, 1029-1038. doi:10.1242/dev.028415

Cai, K. Q., Capo-Chichi, C. D., Rula, M. E., Yang, D.-H. and Xu, X.-X. (2008). Dynamic GATA6 expression in primitive endoderm formation and maturation in early mouse embryogenesis. *Dev. Dyn.* **237**, 2820-2829. doi:10.1002/dvdy.21703

Cheng, P., Andersen, P., Hassel, D., Kaynak, B. L., Limphong, P., Juergensen, L., Kwon, C. and Srivastava, D. (2013). Fibronectin mediates mesendodermal cell fate decisions. *Development* **140**, 2587-2596. doi:10.1242/dev.089052

Choi, E., Kraus, M. R.-C., Lemaire, L. A., Yoshimoto, M., Vemula, S., Potter, L. A., Manduchi, E., Stoeckert, C. J., Jr, Grapin-Botton, A. and Magnuson, M. A. (2012). Dual lineage-specific expression of Sox17 during mouse embryogenesis. *Stem Cells* **30**, 2297-2308. doi:10.1002/stem.1192

Etoc, F., Metzger, J., Ruzo, A., Kirst, C., Yoney, A., Ozair, M. Z., Brivanlou, A. H. and Siggia, E. D. (2016). A balance between secreted inhibitors and edge sensing controls gastruloid self-organization. *Dev. Cell* **39**, 302-315. doi:10.1016/j.devcel.2016.09.016

Evans, A. L., Faial, T., Gilchrist, M. J., Down, T., Vallier, L., Pedersen, R. A., Wardle, F. C. and Smith, J. C. (2012). Genomic targets of Brachyury (T) in differentiating mouse embryonic stem cells. *PLoS ONE* **7**, e33346. doi:10.1371/journal.pone.0033346

Fehling, H. J., Lacaud, G., Kubo, A., Kennedy, M., Robertson, S., Keller, G. and Kouskoff, V. (2003). Tracking mesoderm induction and its specification to the hemangioblast during embryonic stem cell differentiation. *Development* **130**, 4217-4227. doi:10.1242/dev.00589

Gadue, P., Huber, T. L., Paddison, P. J. and Keller, G. M. (2006). Wnt and TGF-beta signaling are required for the induction of an in vitro model of primitive streak formation using embryonic stem cells. *Proc. Natl. Acad. Sci. USA* **103**, 16806-16811. doi:10.1073/pnas.0603916103

Habib, S. J., Chen, B.-C., Tsai, F.-C., Anastassiadis, K., Meyer, T., Betzig, E. and Nusse, R. (2013). A localized Wnt signal orients asymmetric stem cell division in vitro. *Science* **339**, 1445-1448. doi:10.1126/science.1231077

Harrison, S. E., Sozen, B., Christodoulou, N., Kyprianou, C. and Zernicka-Goetz, M. (2017). Assembly of embryonic and extraembryonic stem cells to mimic embryogenesis in vitro. *Science* **356**, eaal1810. doi:10.1126/science.aal1810

Hiramatsu, R., Matsuoka, T., Kimura-Yoshida, C., Han, S.-W., Mochida, K., Adachi, T., Takayama, S. and Matsuo, I. (2013). External mechanical cues trigger the establishment of the anterior-posterior axis in early mouse embryos. *Dev. Cell* **27**, 131-144. doi:10.1016/j.devcel.2013.09.026

Kubo, A., Shinozaki, K., Shannon, J. M., Kouskoff, V., Kennedy, M., Woo, S., Fehling, H. J. and Keller, G. (2004). Development of definitive endoderm from embryonic stem cells in culture. *Development* **131**, 1651-1662. doi:10.1242/dev.01044

Morgani, S. M., Metzger, J. J., Nichols, J., Siggia, E. D. and Hadjantonakis, A.-K. (2018). Micropattern differentiation of mouse pluripotent stem cells recapitulates embryo regionalized cell fate patterning. *eLife* **7**, e32839. doi:10.7554/eLife.32839

Poh, Y.-C., Chen, J., Hong, Y., Yi, H., Zhang, S., Chen, J., Wu, D. C., Wang, L., Jia, Q., Singh, R. et al. (2014). Generation of organized germ layers from a single mouse embryonic stem cell. *Nat. Commun.* **5**, 4000. doi:10.1038/ncomms5000

Pukhlyakova, E., Aman, A. J., Elsayad, K. and Technau, U. (2018). beta-Catenin-dependent mechanotransduction dates back to the common ancestor of Cnidaria and Bilateria. *Proc. Natl. Acad. Sci. USA* **115**, 6231-6236. doi:10.1073/pnas.1713682115

Robertson, E. J. (2005). Making heads and tails of the early mouse embryo. *Harvey Lect.* **101**, 59-73.

Sawada, A., Nishizaki, Y., Sato, H., Yada, Y., Nakayama, R., Yamamoto, S., Nishioka, N., Kondoh, H. and Sasaki, H. (2005). Tead proteins activate the Foxa2 enhancer in the node in cooperation with a second factor. *Development* **132**, 4719-4729. doi:10.1242/dev.02059

Scialdone, A., Tanaka, Y., Jawaid, W., Moignard, V., Wilson, N. K., Macaulay, I. C., Marioni, J. C. and Göttgens, B. (2016). Resolving early mesoderm diversification through single-cell expression profiling. *Nature* **535**, 289-293. doi:10.1038/nature18633

Serup, P., Gustavsen, C., Klein, T., Potter, L. A., Lin, R., Mullapudi, N., Wandzioch, E., Hines, A., Davis, A., Bruun, C. et al. (2012). Partial promoter substitutions generating transcriptional sentinels of diverse signaling pathways in embryonic stem cells and mice. *Dis. Model. Mech.* **5**, 956-966. doi:10.1242/dmm.009696

Siggia, E. D. and Warmflash, A. (2018). Modeling mammalian gastrulation with embryonic stem cells. *Curr. Top. Dev. Biol.* **129**, 1-23. doi:10.1016/bs.ctdb.2018.03.001

Sozen, B., Amadei, G., Cox, A., Wang, R., Na, E., Czukiewska, S., Chappell, L., Voet, T., Michel, G., Jing, N. et al. (2018). Self-assembly of embryonic and two extra-embryonic stem cell types into gastrulating embryo-like structures. *Nat. Cell Biol.* **20**, 979-989. doi:10.1038/s41556-018-0147-7

Tada, S., Era, T., Furusawa, C., Sakurai, H., Nishikawa, S., Kinoshita, M., Nakao, K., Chiba, T. and Nishikawa, S. (2005). Characterization of mesendoderm: a diverging point of the definitive endoderm and mesoderm in embryonic stem cell differentiation culture. *Development* **132**, 4363-4374. doi:10.1242/dev.02005

ten Berge, D., Koole, W., Fuerer, C., Fish, M., Eroglu, E. and Nusse, R. (2008). Wnt signaling mediates self-organization and axis formation in embryoid bodies. *Cell Stem Cell* **3**, 508-518. doi:10.1016/j.stem.2008.09.013

Thomson, M., Liu, S. J., Zou, L.-N., Smith, Z., Meissner, A. and Ramanathan, S. (2011). Pluripotency factors in embryonic stem cells regulate differentiation into germ layers. *Cell* **145**, 875-889. doi:10.1016/j.cell.2011.05.017

Turner, D. A., Rué, P., Mackenzie, J. P., Davies, E. and Martinez Arias, A. (2014). Brachyury cooperates with Wnt/beta-catenin signalling to elicit primitive-streak-like behaviour in differentiating mouse embryonic stem cells. *BMC Biol.* **12**, 63. doi:10.1186/s12915-014-0063-7

Turner, D. A., Girgin, M., Alonso-Crisostomo, L., Trivedi, V., Baillie-Johnson, P., Glodowski, C. R., Hayward, P. C., Collignon, J., Gustavsen, C., Serup, P. et al. (2017). Anteroposterior polarity and elongation in the absence of extra-embryonic tissues and of spatially localised signalling in gastruloids: mammalian embryonic organoids. *Development* **144**, 3894-3906. doi:10.1242/dev.150391

van den Brink, S. C., Baillie-Johnson, P., Balayo, T., Hadjantonakis, A.-K., Nowotschin, S., Turner, D. A. and Martinez Arias, A. (2014). Symmetry breaking, germ layer specification and axial organisation in aggregates of mouse embryonic stem cells. *Development* **141**, 4231-4242. doi:10.1242/dev.113001

Warmflash, A., Sorre, B., Etoc, F., Siggia, E. D. and Brivanlou, A. H. (2014). A method to recapitulate early embryonic spatial patterning in human embryonic stem cells. *Nat. Methods* **11**, 847-854. doi:10.1038/nmeth.3016

Yamaguchi, T. P., Takada, S., Yoshikawa, Y., Wu, N. and McMahon, A. P. (1999). T (Brachyury) is a direct target of Wnt3a during paraxial mesoderm specification. *Genes Dev.* **13**, 3185-3190. doi:10.1101/gad.13.24.3185

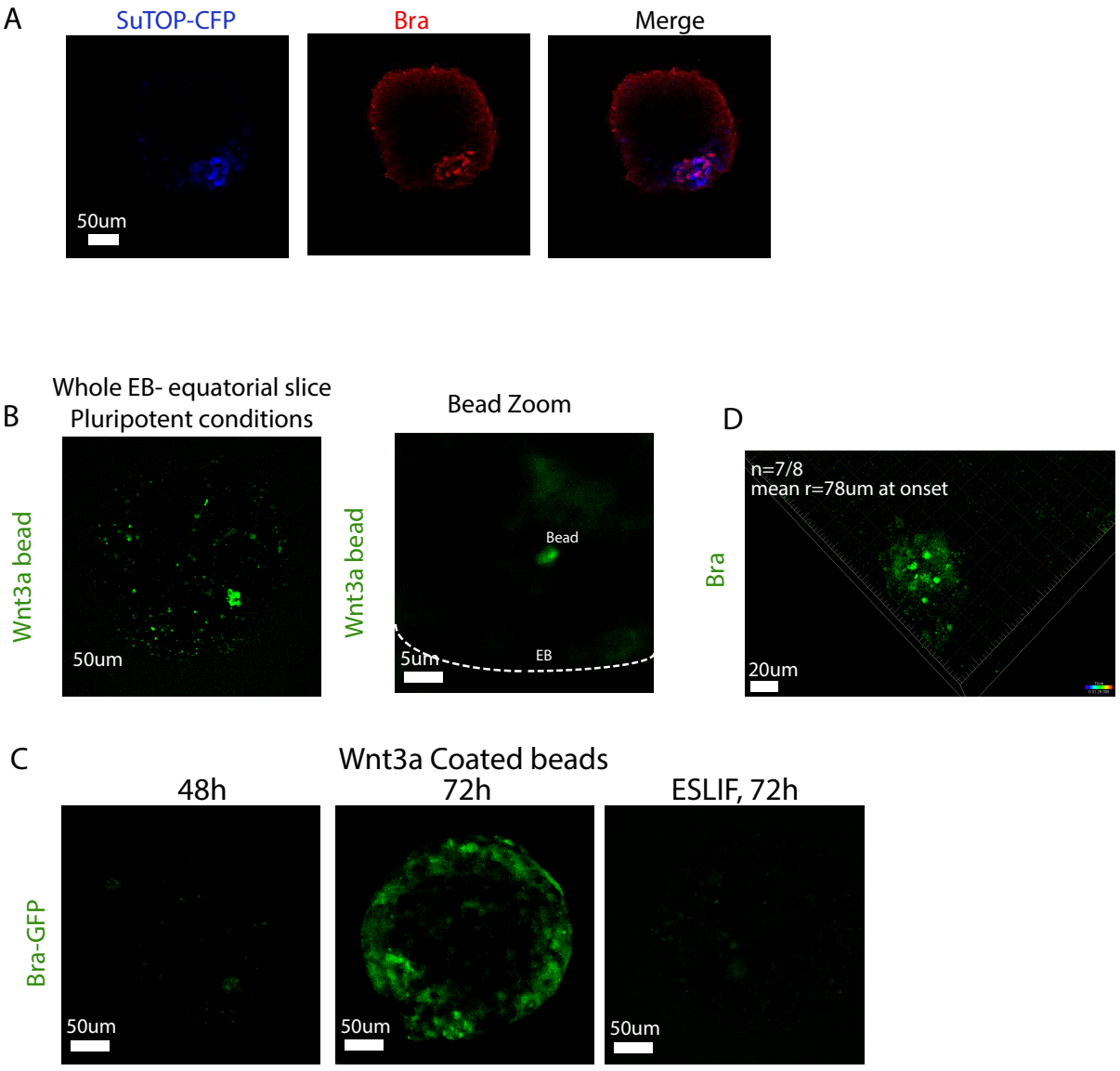

Fig S1. Wnt3a beads integration and small-EB isotropic onset. (A) Bra co-localizes with canonical Wnt response in SuTOP-CFP cells. (B) Left: An equatorial slice of an EB embedded with multiple Wnt3a-coated beads (green). Right: A zoom in snapshot on a Wnt3a-coated bead. (C) Wnt3a-coated embedded beads have no effect on Bra onset in pluripotent conditions (right) or in early differentiation (left), however onset is isotropical on the shell at 72 hrs. (D) An example small EB differentiated in microwells at 72 hrs from aggregation, showing isotropic (spatially uniform) Bra expression onset. The isotropic pattern occurred in 7/8 small EBs (radius at onset = 78+-10um)

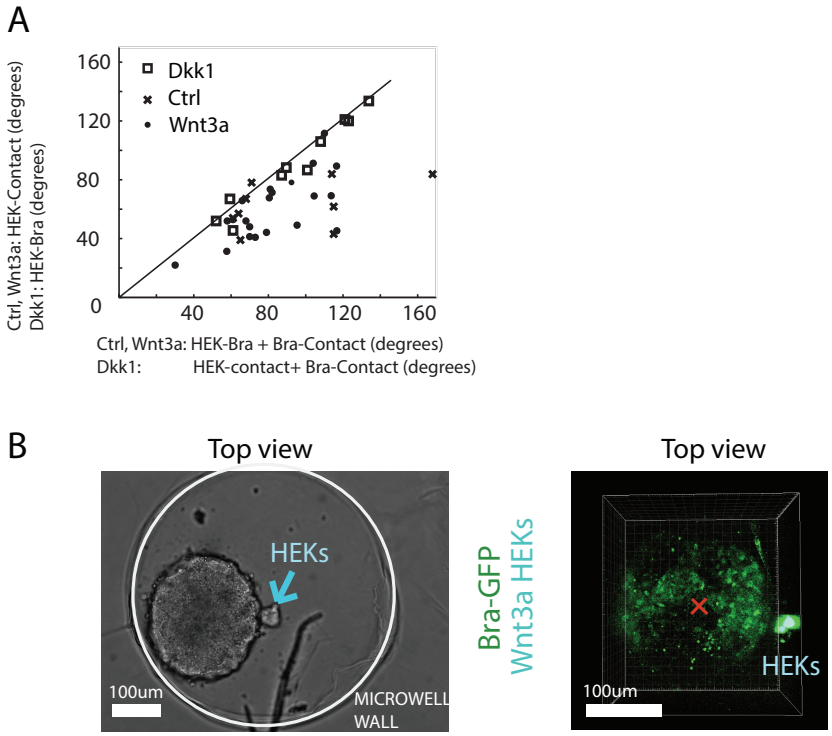

Fig S2. Wnt3a/Dkk1 source, Bra locus, and contact point show high co-planarity. (A) The angle between HEKs signal source and contact (δ, Y-axis) vs. the sum of the angle between HEKs to Bra locus and the angle between Bra locus and contact ($\theta+\varphi$, X-axis) for all EBs quantified in Fig. 4E,F. For EBs harboring Dkk1 or Wnt3a producing HEKs, δ is approximately equal to $\theta+\varphi$, indicating that Bra locus inhabits the same plane defined by the HEKs, contact point and the EB centroid. As expected, in control EBs there is a larger deviation from co-planarity, as the Bra locus is not constrained to that same plane. (B) An example of double Bra loci, one triggered by localized Wnt signaling and the other from contact with the microwell wall.

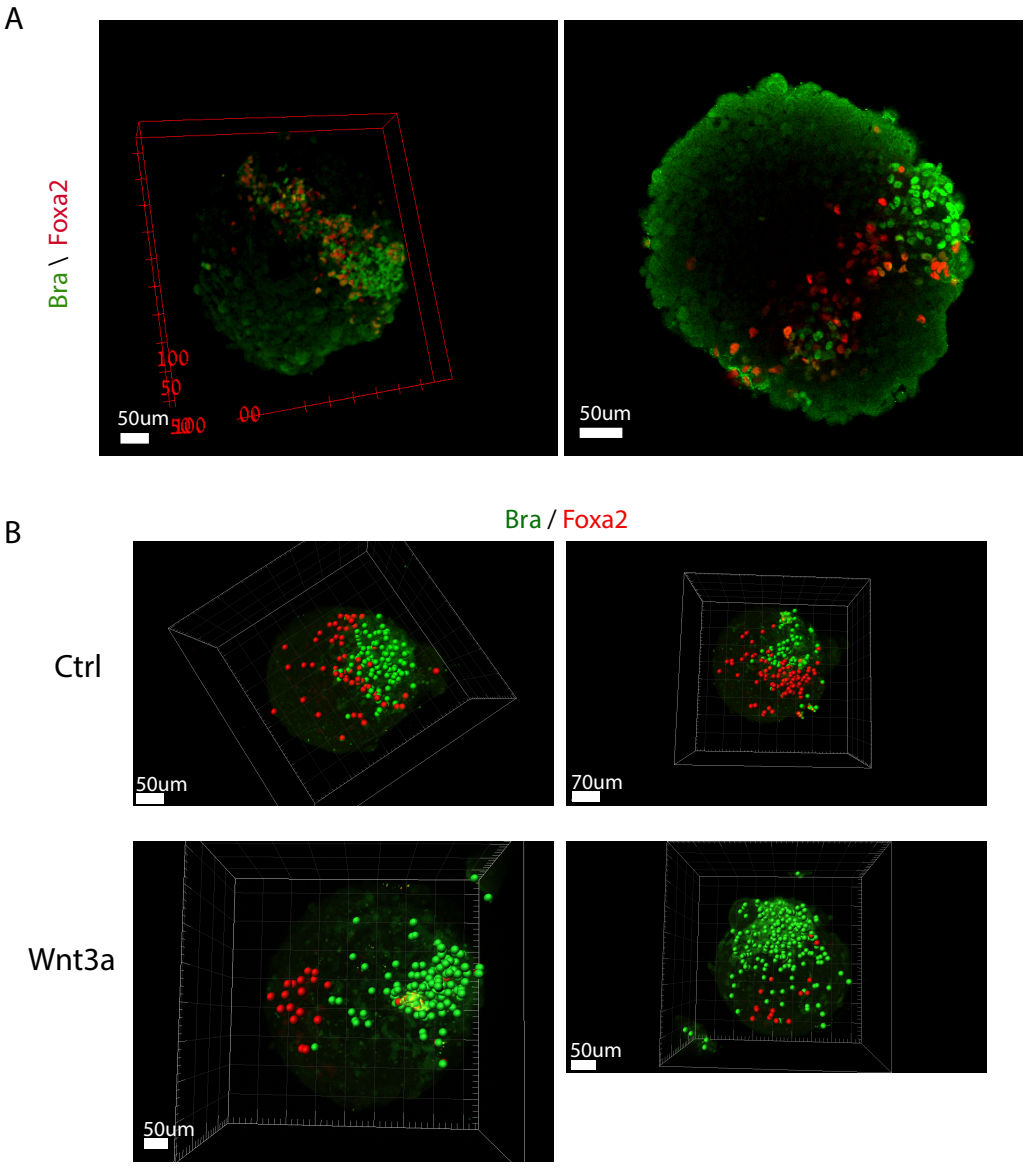

Fig S3. Bra and Foxa2 are spatially adjacent in EBs but can be decoupled by external Wnt signaling. (A) Immunostaining of Foxa2 and Bra at 72 hrs from aggregation. Foxa2 spatially correlates with Bra expression. (B) Segmentation of immunostained Foxa2 (red) and Bra (green) expressing cells at 72 hrs from aggregation. Foxa2 is adjacent to Bra locus in wild type EBs, while Wnt3a treated EBs show Foxa2 downregulation and spatial decoupling from Bra.

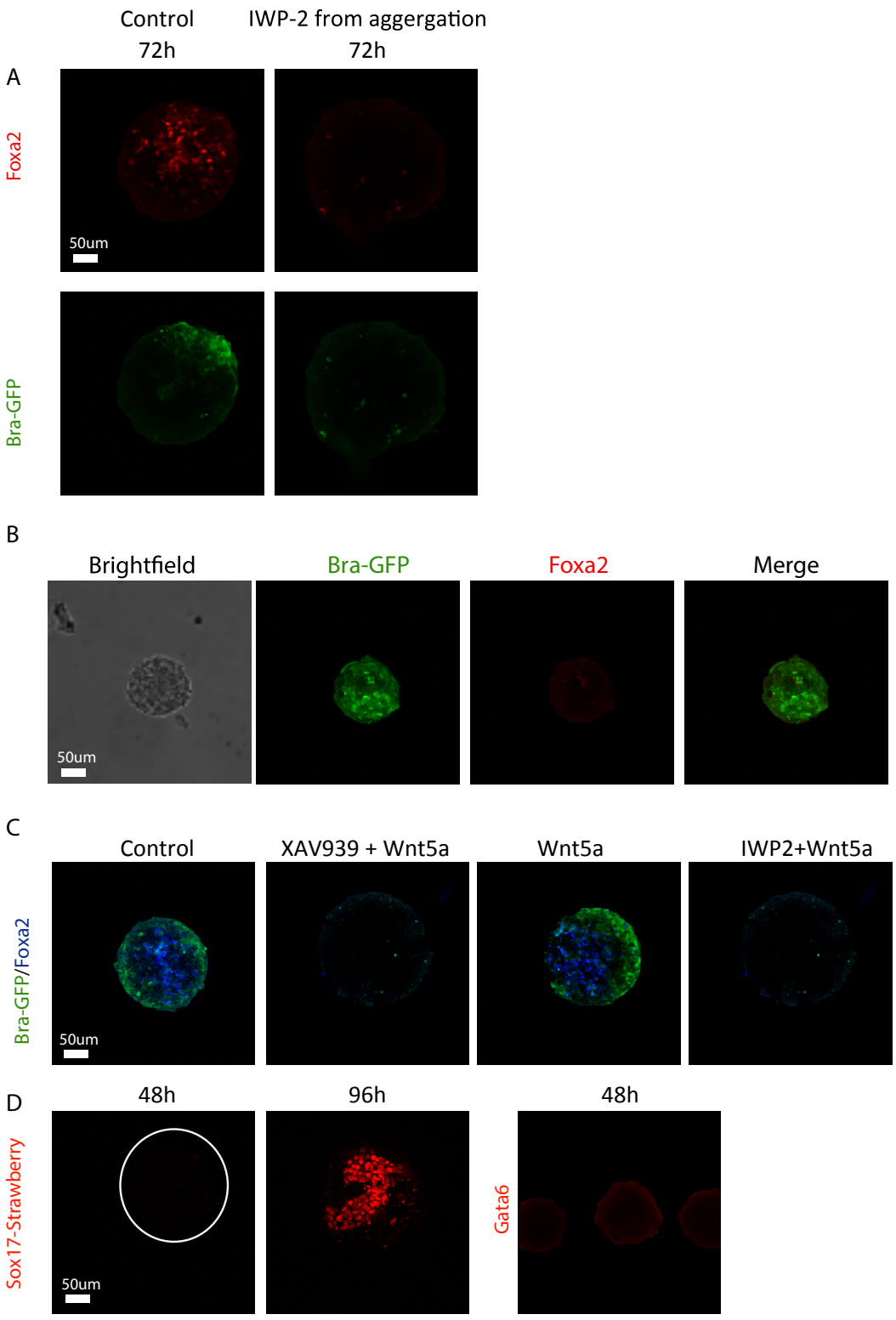

Fig S4. Foxa2 expression abolished under IWP-2 treatment or in small sized EBs. (A) Bra and Foxa2 are not expressed at 72 hrs under IWP-2 perturbation starting at 0 hrs from aggregation. (B) Small size EBs do not express Foxa2 at 72 hrs. (C) Foxa2 and Bra are not expressed under canonical Wnt inhibition (XAV939) or general Wnt inhibition (IWP2), and are not rescued by non-canonical Wnt activation (Wnt5a). (D) Sox17 and Gata6 are not expressed before Bra onset, indicating Foxa2+ cells at 48 hrs do not represent an endodermal lineage.

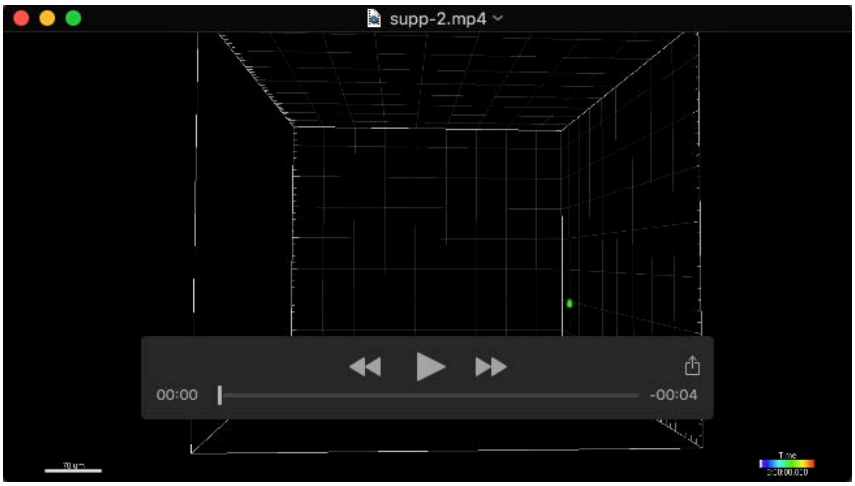

Movie 1 Three-dimensional time-lapse imaging of Bra-GFP in two E14 Bra-GFP embryoid bodies, imaged in microwells between 60 and 96 hrs from aggregation and transfer to differentiation medium. Bra-GFP expression onsets at the bottom (contact point with the glass) , and expands upwards on the outer shell.

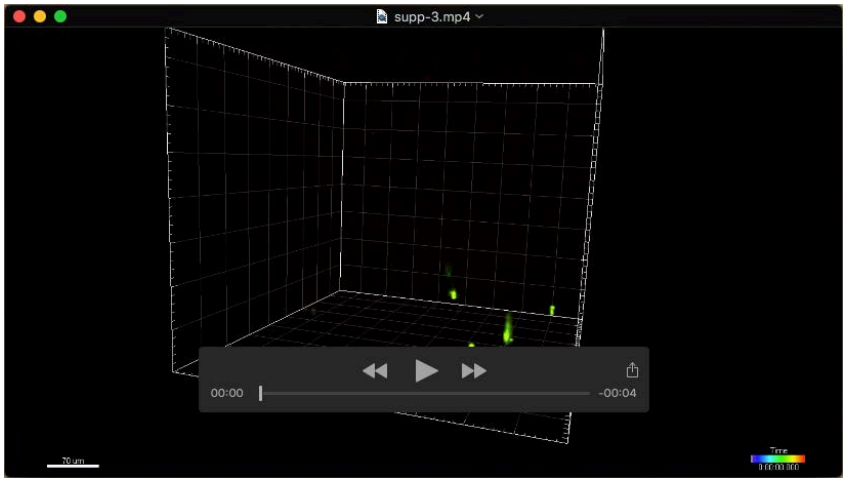

Movie 2 Three-dimensional time-lapse imaging of Bra-GFP in two E14 Bra-GFP embryoid bodies, imaged in microwells between 60 and 96 hrs from aggregation and transfer to differentiation medium. Bra-GFP expression onsets at the bottom (contact point with the glass) , and expands upwards on the outer shell.

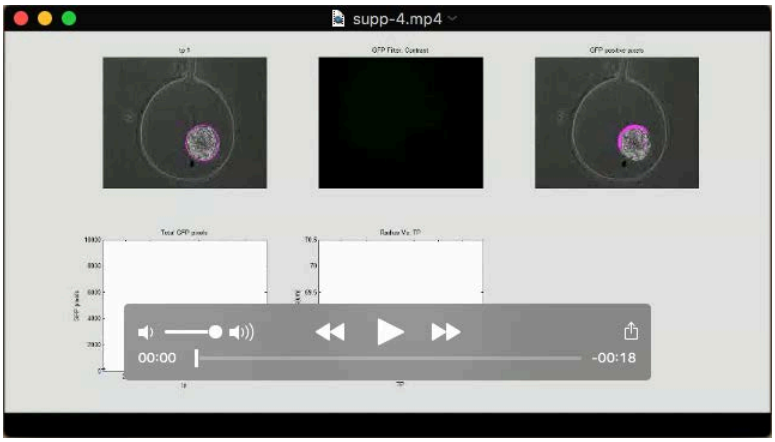

Movie 3 Epifluorescence time-lapse of a Bra-GFP embryoid body, where Bra onset occurred at the bottom. The EB is imaged between 24 and 90 hrs from aggregation, where at 24 hrs it was transferred to a microwell. Top row: left - brightfield imaging of the EB with its encompassing perimeter; center - Bra-GFP; right – overlay of brightfield and GFP-positive pixels (magenta) . Bottom row: left - total Bra-GFP+ pixels vs. time point (time interval between points – 30 minutes) . Blue line - raw data; red dashed line: alpha filter smoothing; yellow line: Bra onset threshold defined as 500 GFP+ pixels; center – EB radius vs. timepoint. Noise at higher time points is due to manual estimation of radius; right – snapshot of Bra-GFP onset frame.

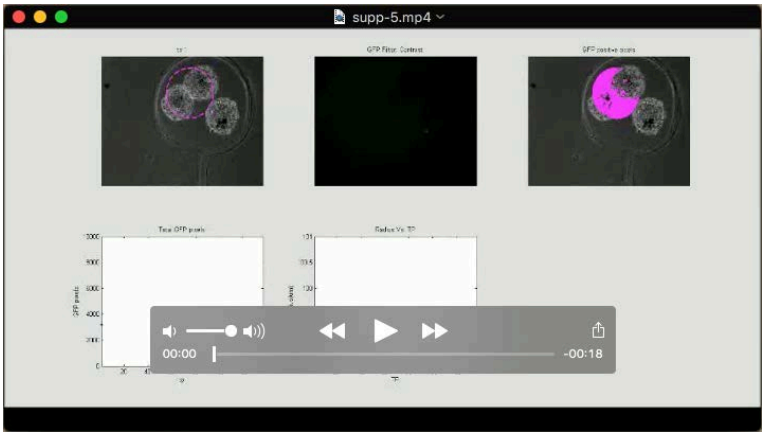

Movie 4 Similar to Movie S3, for a case where Bra expression onset occurred at the contact point with the microwell side. Note in this case the EB originated from 3 smaller EBs that merged together after transfer to the microwell.

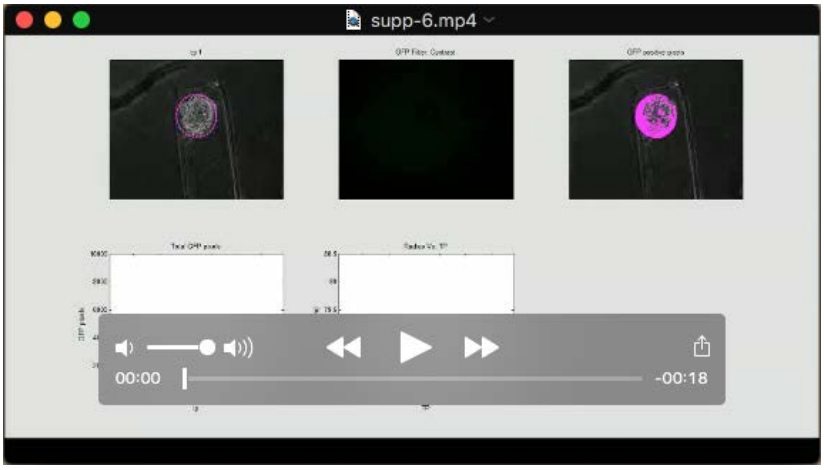

Movie 5 Similar to Movie S3, for an EB differentiated in an elongated micropool (width=200um). In this case, Bra-GFP expression onsets from two different loci (around t.p. 121), at the two sides compressed against the well walls. At t.p. 130 the EB pops out of the channel, resulting in a change in its focus.

Movie 6 Similar to Movie S5, for a case where Bra expression onsets from one of the compressed sides of the EB.

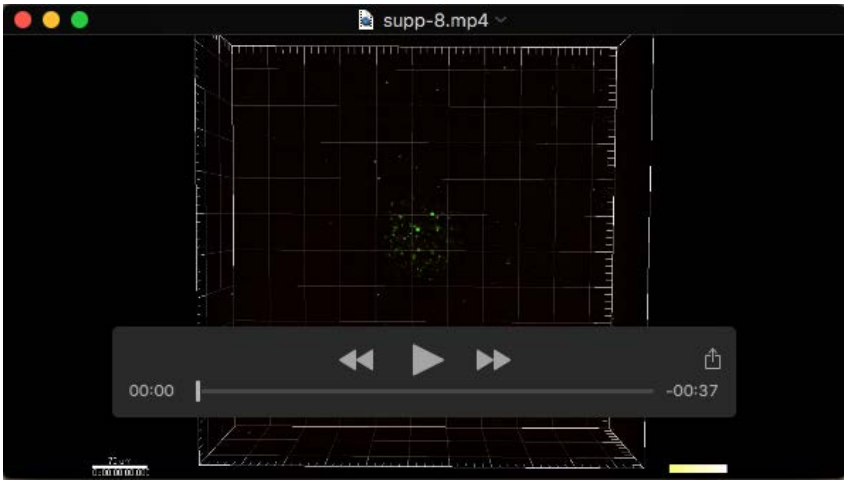

Movie 7 Time lapse of an EB differentiated while embedded in Matrigel. Bra onset occurs uniformly from the whole sphere, representative of the dynamics in 13/15 imaged EBs.

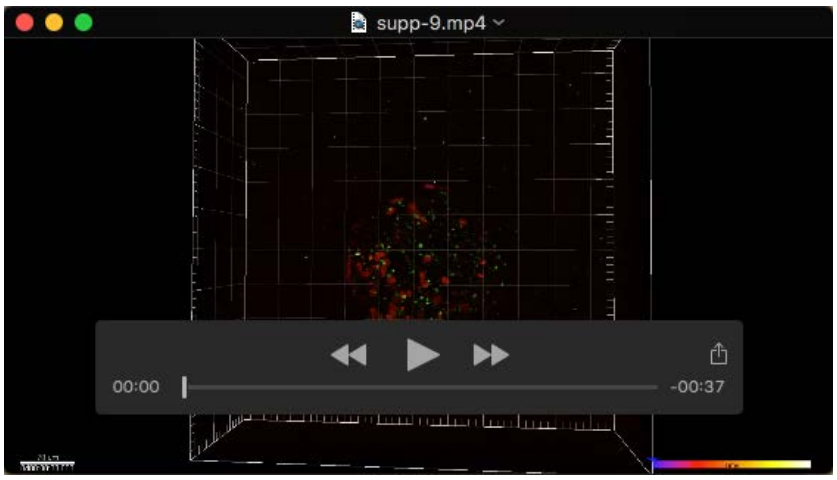

Movie 8 A Bra-GFP, pCMV-Strawberry large EB differentiated while embedded in Matrigel. Bra expression onsets from one locus, expanding from that point into the whole sphere. This dynamic represents 2/15 imaged EBs.